Model evaluation and inter-comparison of surface-level ozone and relevant species in East Asia in the context of MICS-Asia phase III Part I: overview

Jie Li[1,2,3], Tatsuya Nagashima[4], Lei Kong[1,2], Baozhu Ge[1,2,3], Kazuyo Yamaji[5], Joshua S. Fu[6], Xuemei Wang[7], Qi Fan[8], Syuichi Itahashi[9], Hyo-Jung Lee[10], Cheol-Hee Kim[10], Chuan-Yao Lin[11], Meigen Zhang[1,2,3], Zhining Tao[12], Mizuo Kajino[13,14], Hong Liao[15], Meng Li[16], Jung-Hun Woo[10], Jun-ichi Kurokawa[17], Qizhong Wu[18], Hajime Akimoto[4], Gregory R. Carmichael[19] and Zifa Wang[1,2,3]

[1]LAPC, Institute of Atmospheric Physics, Chinese Academy of Sciences, Beijing, 100029, China
[2]College of Earth Sciences, University of Chinese Academy of Sciences, Beijing, 100049, China
[3]Center for Excellence in Urban Atmospheric Environment, Institute of Urban Environment, Chinese Academy of Sciences, Xiamen, 361021, China
[4]National Institute for Environmental Studies, Onogawa, Tsukuba, 305-8506, Japan
[5]Graduate School of Maritime Sciences, Kobe University, Kobe, 657-8501, Japan
[6]Department of Civil and Environmental Engineering, University of Tennessee, Knoxville, TN, 37996, USA
[7]Institute for Environment and Climate Research, Jinan University, Guangzhou, 510632, China
[8]School of Atmospheric Sciences, Sun Yat-sen University, Guangzhou, 510275, China
[9]Central Research Institute of Electric Power Industry, Tokyo, 100-8126, Japan
[10]Department of Atmospheric Sciences, Pusan National University, Pusan, 46241, South Korea
[11]Research Center for Environmental Changes/Academia Sinica, 11529, Taipei
[12]Universities Space Research Association, Columbia, MD, 21046, USA
[13]Meteorological Research Institute, Tsukuba,305-8506, Japan
[14]Faculty of Life and Environmental Sciences, University of Tsukuba, Tsukuba, 305-8506, Japan
[15]Jiangsu Key Laboratory of Atmospheric Environment Monitoring and Pollution Control, Jiangsu Collaborative Innovation Center of Atmospheric Environment and Equipment Technology, School of Environmental Science and Engineering, Nanjing University of Information Science & Technology, Nanjing, 210044, China
[16]Ministry of Education Key Laboratory for Earth System Modeling, Department of Earth System Science, Tsinghua University, Beijing, 100084, China
[17]Japan Environmental Sanitation Center, Asia Center for Air Pollution Research, Niigata, 950-2144, Japan
[18]Beijing Normal University, Beijing, 100875, China
[19]Center for Global and Regional Environmental Research, University of Iowa, Iowa City, IA, 52242, USA

Correspondence to: Jie Li (lijie8074@mail.iap.ac.cn)

Abstract: Long-term ozone (O_3) and nitrogen oxide (NO_x) from fourteen state-of-the-art chemical transport models (CTMs) are evaluated and intercompared to O_3 observations in East Asia, within the framework of the Model Inter−Comparison Study for Asia phase III (MICS-ASIA III), designed to evaluate the capabilities and uncertainties of current CTMs simulations in Asia and provide multi-model estimates of pollutant distributions. These models were run by fourteen independent groups working in China, Japan, South Korea, the United States and other countries/regions. Compared with MICS-Asia II, the evaluation against observations was extended to be one-full year in China and the western Pacific Rim from four months and the western Pacific Rim. In general, the model performance levels for O_3 varied widely, depending on region and seasons. Most models captured the key pattern of monthly and diurnal variation of surface O_3 and its precursors in North China Plain and western Pacific Rim, but failed in Pearl River Delta. A significant overestimation of surface O_3 was evident in May-September/October and January-May over the North China Plain, western Pacific Rim and Pearl River Delta. Comparison with observations revealed that underestimation on dry deposition velocities and large diversity of photochemical production partly contributed to this overestimation and large intermodel variability on O_3 in North China. In term of O_3 soundings, the ensemble average of models reproduced the vertical structure in western Pacific, but overestimated O_3 below 800 hpa in summer. In industrialized Pearl River Delta, the ensemble average presented an overestimation in the lower troposphere and underestimation in the middle troposphere. The ensemble average of 13 models for O_3 did not always exhibit a superior performance compared to certain individual model, in contrast to its superiority in Europe. This suggested that the spread of ensemble-model values had not represented all uncertainties of O_3 or most models in MICS-Asia III missed key processes. This study improved the performance of modeling O_3 in March at Japanese sites than the previous phase of MICS-Asia（MICS-Asia II）. However, it overpredicted surface O_3 concentrations in western Japan in July, which has not been found in MICS-Asia II. Major challenges still remain in regard to identifying the sources of bias in surface O_3 over East Asia in CTMs.

1. Introduction:

Tropospheric ozone (O_3) is a significant secondary air pollutant produced through thousands of photochemical reactions and detrimental to human health, ecosystems, and climate change as a strong oxidant (WHO, 2005; The Royal Society, 2008). With the fast industrialization and urbanization in the last two decades, O_3 concentration is rising at a higher rate in East Asia than other regions and 30% of the days in megacities (e.g. Beijing, Shanghai Guangzhou in China) exceeds air quality standard of World Health Organization (100 μg/m^3) for 8-hour average surface O_3 concentration (Wang et al.,2017). The high O_3 concentrations received more attention from the public and from policy-makers in East Asia. The Ministry of Environment Japan has imposed stringent measures to reduce traffic emissions since 1990s, and non-methane volatile organic compounds (NMVOCs) and NO_x mixing ratios have decreased by 40-50 % and 51-54 %, respectively (Akimoto et al.,2015). In 2012, China released a new ambient air quality standard in which the 8-hour O_3 maximum was set limits for the first time. However, these measures don't prevent the persistent increase of the ground-level O_3 in East Asia. The average mixing ratio of O_3 increased 20-30% in Japan over the last 20 years (Akimoto et al.,2015). In Chinese megacities, 8-hr O_3 concentrations have increased 10-30 % since 2013 (Wang et al.,2017).

The primary method for detailed evaluation of the effect of air quality policies at the scale of East Asia is numerical air quality modeling. Several global and regional scale CTMs (e.g. GEOS-Chem, CHASER, CMAQ, CAMx, WRF-Chem and NAQPMS) over the past few decades have been developed and widely used to simulate the O_3 formation process and evaluate its control strategies (Streets et al., 2008; Li et al., 2007; 2008; Yamaji et al., 2006； Zhang et al., 2008； Liu et al., 2010; Wang et al., 2013; He et al., 2017; Nagashima et al.,2017). These simulations have identified the key precursors of O_3 formation in East Asia (Zhang et al.,2008; Liu et al., 2010; Tang et al., 2011; He et al., 2017), assessed the contributions of international and regional transport (Streets et al., 2008; Li et al., 2008), and predicted the O_3 mixing ratios in different future emission scenarios (Wang et al., 2013). However, discrepancies remain between models and observations, indicating that model simulations of O_3 in East Asia still need to be improved (Han et al., 2008). Modeling uncertainties related to the emissions, chemistry, wet and dry deposition, and transport can hardly be handled using one single model. Model inter-comparison has thus been recognized as an effective way to address problems and has been successfully applied in Europe

and North America in the phase 2 of the Air Quality Model Evaluation International Initiative (AQME II; Rao et al., 2011). Limited model inter-comparison related to air quality in East Asia has been conducted. Phases I and II of the Model Inter−Comparison Study for Asia (MICS-Asia) were initiated in 1998 and 2003, and to explore the potential sources of model uncertainties regarding sulfur, O_3, nitrogen compounds and aerosols (Carmichael et al., 2002, 2008). They found that the predicted temporal variations of surface O_3 in eight regional CTMs generally tended to be lower than that observed in 2001 with poor correlations in the western Pacific in March and December (Han et al., 2008). Model performance levels for O_3 varied largely in southern China. The inconsistency of horizontal grids, emissions and meteorological inputs among models increased the difficulty of explaining intermodel variability in the MICS-Asia II. More importantly, model evaluation in industrialized China has not been conducted because of few observations, which has been detrimental to efforts to improve model performance levels on O_3.

Recently, regional CTMs have been greatly improved by coupling more mechanisms (e.g. heterogeneous chemistry and on-line calculation of photolysis rates) and accurate chemical reaction rates. For example, the gas-phase chemistry mechanisms in Models 3-Community Multiscale Air Quality (CMAQ) have been developed into CBM05 and SAPRC07 from CB04 and SAPRC99. It is critical to evaluate the updated models' abilities for simulating current air quality over East Asia. In 2010, MICS-Asia was expanded to Phase III, in which 13 regional CTMs and 1 global CTM are run over one-full year by 14 independent groups from East Asia and North America, under a common reference model input data set (namely, the emission inventory, meteorological fields and horizontal grids). In addition to observations made in Japan by the Acid Deposition Monitoring Network in East Asia (EANET) that were used in MICS-Asia II, new observational data from China were made available for MICS-Asia III, which were obtained from the Chinese Ecosystem Research Network (CERN) and the Pearl River Delta Regional Air Quality Monitoring Network (PRD RAQMN). An intercomparison of CTMs in China, Japan and western Pacific over one full year has never been performed, which provided a wider database to use in the comparisons. The completeness of MICS-Asia III is therefore unique.

In this paper, we mainly evaluate the abilities of participating models in MICS-Asia III for simulating the concentration of O_3 and its related species in the framework of MICS-Asia III. Several

questions are addressed: (1) What is the performance level of various air quality models for simulating O_3 in East Asia? (2) How consistent or discrepant are the models? (3) How do muti-model ensembles improve the simulation accuracy for O_3? This paper is expected to provide valuable insights into the abilities and limitations of CTMs in East Asia.

2. Models and data

2.1 Experimental set up

In this study, all participating models were run for the year 2010 and provide gridded monthly mean diurnal O_3 and its precursors mixing ratios in the lowest model layer. For O_3, monthly three-dimensional data were also submitted. If two or more observation sites were in the same grid of model, their mean values will be used to evaluate model performance.

2.2 Participating models and input data

Table 1 summarizes the specifications of participating CTMs. These models include two versions of CMAQ (v4.7.1 and 5.0.2；Byun and Schere, 2006), the Weather Research and Forecasting model coupled with Chemistry (WRF-Chem; http:/www.acd.ucar.edu/wrf-chem), Nested Air Quality Prediction Modeling System (NAQPMS; Li et al.,2007), the Japan Meteorological Agency (JMA)'s non-hydrostatic meteorology-chemistry model (NHM-Chem; Kajino et al., 2012), the NASA-Unified Weather Research and Forecasting (NU-WRF; Tao et al.,2013) and GEOS-Chem (http://acmg.seas.harvard.edu/geos/). They have been documented in the scientific literature and widely applied in modeling studies over East Asia. Table 1 did not list model names to maintain model anonymity for each participating model. Similar behavior was also found in MICS-Asia II and other model intercomparison projects (e.g. AQME II).

MICS-Asia III participants were provided with a reference meteorological field for the year 2010, generated with the Weather Research and Forecasting Model (WRF) version 3.4.1 model. The domain of meteorological fields is shown in Fig. 1. WRF v3.4.1 are driven by the final analyses dataset (ds083.2) from the National Centers for Environmental Prediction (NCEP), with 1° × 1° resolution and a temporal resolution of 6 h. A four-dimensional data assimilation nudging toward the NCEP dataset was performed

to increase the accuracy of WRF. The horizontal model domain, which is 182 ×172 grids on a Lambert conformal map projection with 45-km horizontal resolution, is shown in Fig. 1. Vertically, the WRF grid structure consists of 40 layers from the surface to the model top (10 hPa.). The standard meteorological fields were applied by the majority of groups. Several other models performed simulations using their own meteorological models (e.g., RAMS-CMAQ and GEOS-Chem). The WRF-Chem utilized the same model (WRF) as the standard meteorological simulation, but they considered the feedback of pollutants to the meteorological fields. Consequently, their meteorological fields are possible slightly different from the standard. GEOS-Chem is driven by the GEOS-5 assimilated meteorological fields from the Goddard Earth Observing System of the NASA Global Modeling Assimilation Office. The couples of meteorological and CTMs vary for each group, likely resulting in a diversified set of model output.

MICS-Asia III provided a set of monthly anthropogenic emission inventory for the year 2010, which is called as MIX (Li et al.,2016). MIX is a mosaic of up-to-date regional and national emission inventories that include Regional Emission inventory in ASia (REAS) version 2.1 for the whole of Asia (Kurokawa et al., 2013), the Multi-resolution Emission Inventory for China (MEIC) developed by Tsinghua University, a high-resolution NH_3 emission inventory by Peking University (Huang et al., 2012), an Indian emission inventory developed by Argonne National Laboratory (ANL-India, Lu et al., 2 011; Lu and Streets, 2012), and the official Korean emission inventory from the Clean Air Policy Support System (CAPSS; Lee et al., 2011). The biogenic emissions are taken from the Model of Emissions of Gases and Aerosols from Nature (MEGAN). Hourly biogenic emissions were obtained for the entire year of 2010 using version 2.04 (Guenther et al., 2006). Biomass burning emissions were processed by re-gridding the Global Fire Emissions Database version 3 (GFEDv3) (0.5 by 0.5 degree). Volcano SO_2 emissions were provided, with a daily temporal resolution by the Asia Center for Air Pollution Research (ACAP). The emission group in MICS-ASIA III directly prepared a gridded inventory according to the configuration of each CTM. NMVOC emissions are spectated into model-ready inputs for three chemical mechanisms: CBMZ, CB05 and SAPRC-99. Weekly and diurnal profiles were also provided. The standard emission inventory was applied by all models. The majority of models employed official suggested vertical and time profiles of pollutants from each sector by the emission group. M13 and M14 made the projection by themselves. More information can be found in the paper of Li et al. (2017) and Gao et al. (2017).

MICS-Asia III also provided two sets of chemical concentrations at the top and lateral boundaries of the model domain, which were derived from the 3-hourly global model outputs for the year 2010. The global models were run by University of Tennessee (http://acmg.seas.harvard.edu/geos/) and Nagoya University (Sudo et al., 2002). GEOS-Chem was run with a 2.5º×2º horizontal resolution and 47 vertical layers and Chemical AGCM for Study of Atmospheric Environment and Radiative Forcing (CHASER) was run with a 2.8º× 2.8º horizontal resolution and 32 vertical layers. Some models made boundary conditions depending on their own previous experience.

2.3 Observational data for O_3

In this study, East Asia has been divided into three sub-regions as shown in Fig. 1. The selection of the sub-regions is based on emissions, climate and observation data coverage. The North China Plain (EA1) and Pearl River Delta (EA2) represent the highly industrialized regions in the mid-latitudes. EA1 have a temperate and tropical continental monsoon climate with marked seasonality, respectively. EA2 is located in the south of China, and is less affected by the continental air masses. EA3 consists of the northwest Pacific and Sea of Japan, and represents the downwind regions of Asian continent with a marine climate.

Hourly O_3 and NO_x observations in the year 2010 in East Asia were obtained from CERN, PRD-RAQMN), and EANET. The CERN was built by the Institute of Atmospheric Physics, Chinese Academy of Sciences and consists of 19 surface stations within an area of 500 × 500 km^2 in North China Plain (EA1 sub-region; Ji et al., 2012). These stations were set up according to the United States Environmental Protection Agency method designations. Half of them were remote, rural or suburban and clear urban sites. 9 sites were located in the meteorological stations or campuses of universities in urban regions, with little influence from local sources and sinks. The comparison of NO emission rates at these sites in 45km and 3km resolution emission inventories showed that observation generally represented the ~45 km averages of pollutants. The PRD RAQMN was jointly established by the governments of the Guangdong Province and the Hong Kong Special Administrative Region and consists of 16 automatic air quality monitoring stations across the EA2 sub-region (Zhong et al., 2013). Thirteen of these stations are operated by the Environmental Monitoring Centers in Guangdong Province and the other three are located in Hong Kong and are managed by the Hong Kong Environmental Pollution Department. The

PRD RAQMN was to probe the regional air quality, assess the effectiveness of emission reduction measures and enhance the roles of monitoring networks in characterizing regional air quality and supporting air quality management. So, sites are rarely influenced by local sources and sinks. The EANET was launched in 1998 to address acid deposition problems in East Asia, following the model of the Cooperative Program for Monitoring and Evaluation of the Long-Range Transmission of Air Pollutants in Europe. In this study, eight remote stations in the northwest Pacific and Japan (EA3 sub-region) were selected for use in evaluating the model performance level in the downwind regions of the Asian continent (Ban et al., 2016). More information on the EANET can be found at http://www.eanet.asia/. Note that only stations with at least 75% data validity were chosen. Table S1 in the supplements lists detailed site description.

The O_3 and NO_x instruments were an ultraviolet photometric analyzer (model49i, Thermo Fisher Scientific (Thermo), USA) and a chemiluminescence analyzer (model42iTL, Thermo, USA), respectively. NO_x measurement existed sometimes biases (especially for stations far from sources) when using molybden convertors devices since all nitrogen oxydes are measured. A one-month continuous measurement in August by a chemiluminescence analyzer and Aerodyne Cavity Attenuated Phase Shift Spectroscopy (CAPS) showed that this bias from a chemiluminescence analyzer was small when NO_2 concentrations were more than 10-15 ppbv, and ranged from 10% to 30% under low NO_2 (<10 ppbv) (Ge et al., 2013).

3. Model validation and general statistics

3.1 Annual concentrations of surface O_3, nitric oxide (NO) and nitrogen dioxide (NO_2)

Fig. 2 provides a concise comparison of model performance on annual O_3, NO and NO_2 in three sub regions in East Asia. A box-and-whisker representation was used to show the frequency distribution of monthly concentrations at stations in each sub-region. The O_3 normalized mean bias (NMB) and root mean square error (RMSE) of ensemble mean were significantly less than the ensemble median in most situations (Table 1). Therefore, we only presented the results of multi-model mean ensemble (Ense). In general, the majority of models significantly overestimated annual surface O_3 compared with the observations in EA1, EA2 and EA3. Ense overestimated surface O_3 by 10-30 parts per billion volume

(ppbv) in these subregions. Ense NO_2 was close to the observations to within ±20% in all subregions. In EA1 and EA2, Ense NO was 5-10 ppbv lower than observation, while it showed a reasonable performance in EA3.

Among all models, M11 in sub-regions EA1 and EA2, M7 in EA2 and EA3 were closer O_3 observations. M11 simulated O_3 achieved a RMSE of 9.5 ppbv and 13.3 ppbv in EA1 and EA2, respectively (Table 2). The performance levels of models for simulating O_3 were closely related to their performances for NO_2 and NO. In highly polluted regions (EA1 and EA2), a persistent underestimation of NO was evident across most models. An interesting phenomenon was that models' performance regarding O_3 varied greatly in EA3, although they but M8 showed a consistent performance with respect to NO and NO_2. This suggests that O_3 was significantly affected by other factors in addition to local chemistry in EA3. M8 underestimated O_3 and overestimated NO in all sub-regions by 40-50%. The strongest O_3 titration in M8 may result in lower O_3 than other models and observations.

3.2 Monthly variation of surface O_3, NO and NO_2

Fig. 3 presents the monthly mean concentrations of O_3, NO and NO_2 in three sub-regions over East Asia. All models captured the observed seasonal cycles of O_3, NO and NO_2 in EA1. In May-September, Ense O_3 was 10-30 ppbv higher than observations, 30-70% of observed values, while Ense NO and NO_2 appeared to be consistent with observations, attaining mean biases of < 3 ppbv. This suggests that the intercomparison on O_3 production efficiency per NO_x with observations is needed. In EA2, Ense O_3 agreed well with observed high autumn O_3, but overestimated from January to September by 5-15 ppbv (15-60% of observations). This overestimation reached the highest in March-April (15ppbv) and led to a spring peak in simulated O_3 which was not found in observations. This overestimation was partly related to the underestimation of NO in the same months, which decreased the titration effect. For NO_2, Ense agreed well with observed values in June-December, and slightly underestimated observations in January-May. In EA3, the ensemble NO_2 was generally close to the observations to within ±0.5 ppbv. A significant overestimation of O_3 and underestimation of NO existed in June-October. Similar results have been found in MICS-Asia II and other model inter-comparison project under the Task Force on Hemispheric Transport of Air Pollution (TF HTAP), which suggested that such results may stem from

the difference in the representation of dispersion by southwesterly clean marine air masses in different metrological fields used in CTMs (Han et al.,2008; Fiore et al., 2009).

For individual models, M11 achieved the best model reproductivity of monthly mean O_3 in EA1 among models.. Other most models overestimated O_3 by 100-200% in May-October. The largest model bias and intermodel variability for NO and NO_2 appeared in winter, which likely came from the NO_x vertical diffusion and heterogeneous chemistry (Akimoto et al., 2019). In EA2, M7 seems to have achieved the best reproducibility for O_3. Most models (except M11 and M12) exhibited high O_3 concentrations in March-May and September-November. Observed O_3 showed that the highest concentrations appeared in October-November. M11 captured the observed January-May O_3 because of relatively high NO concentrations. However, NO was overestimated by M11 in May-September, which led to the underestimation of O_3. In EA3, spatially averaged O_3 concentrations often differ by more than 20 ppbv in the individual models. The highest intermodel variability on O_3 appeared in May-October, which overestimated O_3 in comparison to observations by 10-40 ppbv. Interestingly, although M8, M9 and M14 exhibited a similar magnitude with observations in June-September, they significantly underestimated observations in other months by 200-300%. A detailed investigation is required in future studies.

3.3 Diurnal concentrations of surface O_3

Sub-regional O_3 diurnal variations are shown in Fig. 4. In general, model results for three sub-regions exhibited a larger spread with a magnitude of 10-50 ppbv throughout the diurnal cycle than that in Europe and North America (Solazzo et al., 2012). The Ense O_3 in summer exhibited a systematic overestimation (20 ppbv) throughout the diurnal cycle in EA1.This indicated that models had difficulty dealing with summer O_3 in North China Plain. Compared with summer, there was only a slight systematic overestimation of Ense O_3 in other seasons (3-5 ppbv). In EA2, Ense O_3 generally agreed with the observations in summer, autumn and winter. In particular, the O_3 maximum around noon was reproduced, reasonably. There was only a 3-5 ppbv overestimation during 16:00-23:00 and early morning (6:00-10:00). In spring, a systematic overestimation of Ense O_3 exited in the whole diurnal cycle (5-10 ppbv). In EA3, Ense captured the small diurnal variation of O_3 in four seasons, but significantly overestimated

observations in summer and autumn (5-20 ppbv). In spring and winter, differences between Ense and observations were within 5 ppbv.

Among all models, M11 exhibited the best model performance level on peak daily O_3 concentrations of 60 ppbv in 14:00-16:00 in EA1, but still overestimated nighttime O_3 by 10 ppbv. Compared with summer, models' performances had a significant improvement in winter because of the weak intensity of photochemical reactions, except M2, M10 and M8. Differences between observations and most simulations in both nighttime and daytime were within 5 ppbv. The contrast of the models' performances between summer and winter implied that the variety of parametrizations on chemistry in different models partly explained the intermodel variability of simulated O_3 in EA1 (North China Plain). In EA2, the majority of models agreed well with the diurnal variation in summer and autumn. However, most models had a tendency to overestimate the O_3 concentrations in both daytime and nighttime in spring. The overestimated magnitude exceeded 10 ppbv and 25 ppbv (out of observed values of 20-35 ppbv) in nighttime and daytime, respectively. M11 reproduced the observed O_3 in spring, but underestimated O_3 in summer and autumn. In EA3, the significant intermodel variability still existed throughout the year. The amplitude of intermodel variability except M8 and M14 reached approximately 20 ppbv and approximately 10 ppbv in spring-summer and autumn-winter, respectively. M8 and M14 exhibited the lowest O_3 among models in the whole year.

3.4 Error statistics on surface concentrations

In this section, we present statistics concerning the performance levels of the models based on monthly values. They are calculated by equations in Appendix A. On a yearly basis, all models showed the highest (0.8-0.9) and lowest (0.1-0.6) correlation coefficients for O_3 in EA1 and EA2, respectively (Table 2). The high correlations in EA1 were mainly because the summer-maximum and winter-minimum seasonal cycle is the typical pattern in polluted regions that were well represented in all the participating models. In general, Ense performed a better performance level than individual models for representing NO_2 in East Asia, reproducing the observed seasonal cycle and magnitudes. However, Ense did not always exhibited a superior performance for O_3 over certain individual model in East Asia, which was in contrast to its performance in Europe (Table 1). M7 and M11 agreed well with observations in EA1 and EA2, while ENSE tended to overestimate O_3 concentrations in May-September in EA1 and

January-September in EA2. Loon et al. (2007) indicated that ENSE exhibited a superior performance level only when the spread of ensemble-model values was representative of the uncertainty of O_3. This indicated that most models did not reflect this uncertainty or missed key processes in MICS-Asia III.

The large overestimation of most models in May-September led to high NMB (0.25-1.25) and RMSE (10-33 ppbv) in EA1. M11 had the lowest NMB (0.09) and RMSE (9.46 ppbv) among models. In EA2, M9 and M10 had larger correlations than the other models. However, their NMB and RMSE were also the highest. This implied that systematic model biases existed in these two models. M7 exhibited a lower NMB and RMSE than other models, but its correlation was only 0.29. In EA3, the correlations exhibited the largest intermodel variability among all sub-regions, ranging from -0.13-0.65. M7 showed the lowest NMB and RMSE. This is likely caused by the cancelling effect of its overestimation in summer and underestimation in other seasons (Fig. 3).

For NO, correlations of models in EA1 ranged from 0.57-0.68, which indicated all models did a good job in reproducing the spatial variability of NO in this sub-region (Table 3). The NMBs indicated underestimation by models except M8 which mostly occurred in winter. This underestimation partly was attributed to the coarse model horizontal resolution (45km) used in the MICS-Asia III, which hardly reproduced concentrations of short-lived species. In contrast to most models, M8 overestimated NO concentrations in all three sub-regions. It is noted that observations of NO were too low (<0.3 ppbv) in EA3 to be discussed in this study.

Table 4 shows the statistics of models' performance levels for NO_2. In general, most models exhibited a better performance levels for representing NO_2 than O_3 and NO in EA1. The NMBs ranged from -0.28-0.32, which were much lower than O_3 (0.48-1.25). The correlations were 0.54-0.66, implying the reliable model performance levels for reproducing the spatial and month-to-month variability of NO_2 in EA1. Similar to O_3 and NO, the correlation coefficients of NO_2 in EA2 remained low. Thus, a dedicated investigation on O_3, NO and NO_2 in EA2 is urgent, but beyond the scope of this study. In EA3, correlation coefficients ranged from 0.5-0.72. The NMBs and RMSEs except M8 ranged from -0.42-0.46 and 0.91-1.79 ppbv, respectively.

3.5 Vertical profiles of O_3

Fig. 5 the vertical profiles of observed and simulated O_3 in East Asia in summer and winter. Ensemble means (Ense) presented an underestimation and overestimation for EA2 O_3 in middle (500-800 hpa) and lower (below 900 hpa) troposphere, respectively. In winter, the underestimation was even extended to 200hpa. The magnitudes of underestimation and overestimation reached 10-40 ppbv and 10-20 ppbv, respectively. In EA3, Ense reproduced the vertical structure of ozone in both summer and winter. An overestimation existed below 800 hpa in summer, with a magnitude of 10-20 ppbv.

A large intermodel variability of O_3 above 300 hPa is evident in all sub-regions, which is attributable to the various different top boundary conditions among models. However, this large variability was not transmitted to middle troposphere (400-600 hPa), in which O_3 concentrations were consistent among models. In the lower troposphere, a small intermodel variability in winter appeared below 900 hPa in three sub-regions, and slowly decreased with height. The mean standard deviations of models (σ) below 900 hpa were 7.6 ppbv, 6.9 ppbv and 6.0 ppbv in EA1, EA2 and EA3, which covered 18.3%, 15.0% and 15.4% of mean O_3 concentrations. In 700-900 hpa, σ decreased to 5.4 ppbv, 4.4 ppbv and 4.8 ppbv in EA1, EA2 and EA3, 12.2%, 9.4% and 10.8% of mean O_3 concentrations.

In the lower troposphere, the intermodel variability in summer were generally higher than those in winter. In polluted regions (EA1), σ reached 16.3 ppbv (20.8 % of mean concentrations) in summer, greatly exceeding those in winter (6.2 ppbv, 15.2%). Various vertical structures of O_3 were found below 700 hPa in summer. O_3 concentrations slowly increased with height in M8 and M11, but they mixed well in the PBL and decreased from 800 hPa to 700 hPa in the other models. Akimoto et al. (2019) found that the parameterization on downward O_3 transport from the upper boundary layer contributed a lot to the discrepancy between M1, M6 and M11. In EA2, vertical structures of O_x among models were consistent, but concentrations differed more than those in EA1. σ covered 22% of mean concentrations.

4. Multi-model ensemble O_3 and comparison with MICS-Asia II

4.1 Spatial distribution of single model and multi-model ensemble O_3

Fig. 6 shows that the spatial distributions of MICS-Asia III ensemble mean surface O_3 (Ense) and the coefficient of variation (CV). The CV is defined as the standard deviation of the modeled O_3 divided

by the average. The larger the value of CV, the lower the consistency among the models. In summer, ENSE predicted the elevated O_3 concentration belt in the middle-latitudes (30°-45°N). A region of O_3 in excess of 60 ppbv stretched across North China Plain and China East Sea, which was much higher than values in MICS-Asia II (45-50 ppbv) for the year of 2001 (Han et al.,2008). In other seasons, the O_3 distribution shows higher O_3 over ocean than in eastern China, reflecting the O_3 titration from high NO_x emissions. Due to the stratospheric injection, surface O_3 over Tibet plateau remained a high level in the whole year, ranging from 50 to 65 ppbv. The seasonal cycle of surface O_3 in Ense in MICS-Asia III agreed with that in MICS-Asia II, but O_3 levels in polluted regions were higher (Han et al., 2008).

The CV ranged from 0.1-0.6 in East Asia. The highest values were found in EA1 in winter. These high values in low-latitude western Pacific (10°S-15°N) and Indian Ocean were likely caused by the treatment of lateral boundaries in models. In MICS-Asia III, M7, M8 and M9 employed the default configurations of models, and the others employed outputs of GEOS-Chem/CHASER/MOZART-GOCART global model. Compared with MIC-Asia II, the CVs in Asian continent except winter remained a similar level in this study (0.1-0.3) (Carmichael et al.,2008).

Although all models similarly predicted the elevated summer O_3 concentration belt in the middle-latitudes (30°-45°N), the magnitude of the enhanced O_3 were different among the models (Fig. 7). M5 predicted the highest O_3 concentration of 60-90 ppbv in the North China Plain (EA1) and its outflow pathways including Bohai Sea, East China Sea, Korea, Japan and the Sea of Japan (Locations are shown in Fig. S1 in the supplements), whereas M8 predicted the lowest 35-50 ppbv. Overhang of 30 ppbv contour lines extending into Northwest Pacific in the Asian continent outflow plume differed considerably among models. The plume of 30 ppbv or higher O_3 in M1-M6, M13 and M14 reached further south and east of Japan (135°E, 20°N), than M8, M10 and M11 (120°E, 30°N). In MICS-Asia II and HTAP, differences of frequency of marine air masses from the western Pacific Ocean were thought to be possible cause of O_3 discrepancy over ocean among models because of different meteorological drivers (Han et al., 2008). In MICS-Asia III, the winds fields in models were similar because models the same or similar meteorological fields (Fig. S2 in the supplements). Hence, this inconsistency among models have resulted from the combined influence of a series of factors that included the diversity in condensed gas-chemical mechanism and heterogeneous chemistry. Li et al. (2015) found that the

chemical production was the dominated controlling factor of O_3 along the outflow pathways near the North China Plain in summer, rather than lateral and top boundary conditions. Impact of aerosols on ozone in these regions were frequently reported in Olson et al. (1997) and Li et al. (2018), by altering photolysis rates and heterogeneous chemistry. The detailed comparison on parameterization of these processes in models are needed in future intermodel comparison project in Asia.

In winter, the distribution patterns of O_3 were quite alike among models, with high concentrations over parts of western China, northeastern India and the western Pacific from the East China Sea to south of Japan (Fig. S3 in the supplements). In spring and autumn (Fig. S4 and Fig. S5 in the supplements), O_3 concentrations were generally higher than in winter in the whole model domain because of the enhancement of solar radiation or stratosphere-troposphere exchanging fluxes of O_3. A major feature consistently produced by all models was the enhancement of O_3 over southern Tibet, northeastern India and the western Pacific, which was generally similar to that in winter. The position of O_3 enhancement further north of Japan was comparable with winter.

4.2 Comparison with MICS-Asia II

In MICS-Asia II, model evaluation on O_3 were conducted in only sites in the western Pacific. Fig. 8 presents the simulated and observed surface O_3 at these monitoring sites in the phase II and III of MICS-Asia project. Note that different models were employed in two phases. In general, most models captured the major distribution of O_3 at most sites in both MICS-Asia II and III. ENSE showed a good consistency in March and December of 2001 and 2010. The underestimation of O_3 in March at Japan sites (site 4: Sado-seki, site 5: Oki and site 6: Banryu) in Phase II was largely improved in Phase III. However, the surface O_3 at western Japan (site 4: Oki, site 5: Hedo and site 6: Banryu) were severely overestimated in July 2010 by 10-30 ppbv. This overestimation has not been found in Phase II, in which the difference with observations was approximately 5 ppbv. Rural sites in western Japan were located in the upwind regions of Japanese domestic emissions, and usually used to capture the impact of Asian continent outflows. The overestimated O_3 in North China Plain (EA1) in Phase III contributed a lot to the enhanced concentrations at sites of western Japanese sites in July 2010. This indicated that the transboundary transport from the Asian continent in MCIS-Asia III was likely overestimated compared with that in MICS-Asia II.

5. Discussions

In MICS-Asia II, Han et al. (2008) guessed that the diversity of meteorological fields, dry deposition, PBL, model treatment of chemistry and other physical processes contributed to model biases with observations and the intermodel variability. Quantifying the contribution of these processes is one effective way to explain model biases by sensitivity. But this required a tremendous amount of computational cost for 14 models. A qualitative analysis on potential causes by comparison between models and observations on these processes is essential to narrow sensitivity simulating scenarios for next phase of MICS-Asia. In MICS-Asia III, common input data (emission and meteorology) provide a good chance for this qualitative analysis on model parameterizations. We evaluated the models on dry depositions, PBL and chemistry by collecting their observations (dry deposition velocity and PBLH) as much as possible. This work was not conducted in MICS-Asia II and is believed to be helpful for model developers to improve model performance in East Asia.

5.1 Dry depositions

Previous studies revealed that dry deposition processes are the key net sink of O_3, accounting for about 25% of total removed from the troposphere (Lelieveld and Dentener, 2000). The uncertainty of dry deposition in CTMs is still high because many processes are heavily parameterized in models (Hardacre et al.,2015). In this study, the simulated dry deposition velocities of O_3 were compared. Simulated deposition velocities were calculated from Eq. (1):

$$V_d = F/C \qquad (1)$$

Where F and C represent the simulated dry deposition flux and surface O_3 concentrations, respectively. We determined the spatial mean dry deposition velocities at stations in each sub-region.

Fig. 9 presents the simulated and observed monthly spatial mean dry deposition velocities of O_3. In EA1, ensemble mean values underestimated observed dry deposition velocities of O_3 (v_d) in August-September, but still fell into the range of observed standard deviation. This underestimation could contribute to the overestimation of O_3 concentrations in summer discussed in section 3.2. The lower dry deposition velocities in May-July from M1, M2, M4 and M6 than that of M11 partly explained higher summer surface O_3 from those simulations than that from M11. However, M13 and M14 still produced

high O_3 concentrations in May-September although their dry deposition velocities were similar to that of M11(Fig. 3). This suggested that there were other factors besides dry deposition playing important roles in the overestimation of summer O_3 in EA1. In October-November, simulated v_d apparently overestimated observations by 30-50%.

In EA2, similar features with EA1 are found. M1, M2, M4 and M6 were quite consistent with each other, with a seasonal cycle of spring minimum. M11, M12 and M14 had no obvious seasonal variability, with a magnitude of 0.1-0.2 cm/s. The seasonal pattern in M13 was considerably different from the other models, exhibiting a maximum in April-September with higher dry deposition velocities (0.5 cm/s). The performance of the models for dry deposition velocities was not always consistent with O_3 concentrations. For example, O_3 concentrations in M13 still remained high levels under higher dry deposition velocities conditions.

In EA3, most stations were remote oceanic sites, and few dry deposition observations were conducted. So, we collected observations in other oceanic sites to evaluate model performance (Helmig et al., 2012). Ense of v_d agreed with observations reasonably (Fig. 9). Both observations and simulated v_d showed a July-September maximum with a magnitude of 0.02-0.03 cm/s. Park et al. (2014) revealed that surface O_3 in EA3 were more sensitive to dry deposition parameterization schemes in CTMs. O_3 on oceans differed by 5-15 ppbv in East Asia resulting from different dry deposition parameterization schemes. Thus, more observations are needed over oceans in EA3 to decrease the uncertainties on O_3 simulations.

5.2 Relationships between surface NO_x and O_3

In general, surface O_3 mainly comes from the photochemistry involving NO_x and VOCs in polluted regions. Theoretical and simulation results showed that O_3 production increased almost linearly with the NO_x increase under NO_x-sensitive conditions and remained relatively unchanged or even decreased in NO_x saturated (often called “VOCs-limited”) conditions (Kirchner et al.,2001; Sillman and He et al., 2002; Tang et al., 2010). Recent observations found that regional O_3 in the North China (EA1) and Pearl River Delta (EA2) was changing from NO_x-limited to NO_x-saturated regions (Jin et al., 2015). Examining the O_3-NO_x relationships is a good way of investigating sources of intermodel variability and model

errors concerning on O_3 chemistry in East Asia. Fig. 10 presents the O_3 concentrations as a function of NO_x in May-September based on the monthly daytime (8:00-20:00) mean observed and simulated results at stations shown in Fig. 1.

In EA1 (North China Plain), observations clearly revealed that O_3 concentrations decreased with the increase in NO_x concentration. O_3 concentrations mostly remained high levels (40-60 ppbv) when NO_x was less than 20 ppbv. This implied that O_3 was under NO_x-saturated conditions in EA1 in May-September. The slope and intercept of regression line between O_3 and NO_x were -0.77 ppbv/ppbv and 59.5 ppbv, respectively. Among models, M11 were in relative agreement with observations, reasonably. The slope and intercept (-1.01 ppbv/ppbv, 63.23 ppbv) were close to observations. Other models showed a higher model bias and intermodel variability on relationships between O_3 and NO_x. Their slopes mostly ranged from -1.25 ppbv/ppbv to -2.13 ppbv/ppbv, 1.3-2.8 times of observed slope. Their intercepts were 74.9 -121.2 ppbv, much higher than observation (59.5 ppbv). Akimoto et al. (2019) calculated the net photochemical production of M1, M6 and M11, and found that weak net chemical production in M11 were mostly responsible for low O_3 than M1 and M6. This is consistent with the low slope in M11. Interestingly, M13 maintained a similar O_3 level at all NO_x levels (Slope: -0.09), which was different from other models and previous theoretical results.

In EA2, M1, M2, M4 and M6 reproduced observed O_3 in low NO_x (< 30 ppbv) but failed to capture the low O_3 under high NO_x conditions (30~40 ppbv). This explained the overestimation of these models for O_3 in May-September. By contrast, M8 and M11 produced excessively high NO_x values, which resulted in their underestimation for O_3. In M13 and M14, O_3 concentrations were nearly constant in all levels of NO_x. O_3 was positively correlated with NO_x in M9 and M10, which is in contrast to observations. This suggests that more attention is needed when policy-makers designate the O_3 regime (VOCs-limited or NOx-limited regimes) using M9, M10, M13 and M14.

Stations in EA3 are mostly located over clean oceans or islands. NO_x concentrations were less than 3 ppbv, which indicated the local chemistry appeared to not be a key factor of O_3 formation. Thus, we did not discuss the simulated O_3-NO_x relationship further in this study.

5.3 Other factors

Previous studies revealed that O_3 precursors are mostly constrained within the boundary layer (Quan et al., 2013). The model evaluation on PBLH is essential for the interpretation of model biases with observations. Unfortunately, this evaluation was not conducted in MICS-Asia II. In MICS-Asia III, all selected models exhibited the spring-maximum and winter-minimum season cycle in EA1 (Fig. S6 in the supplements), which captured the major pattern of climatology of PBLH observations (Guo et al.,2016). The Ense on PBLH only overestimated radiosonde measurements by100-200 m (~10-15%). This is likely caused by the inconsistency of samples between models and measurements. The simulation was the mean value of 12 hours (08:00-20:00), while the average of measurements was calculated based on 3 hours (08:00, 14:00 and 20:00). In EA2, observed PBLH did not varied as that in EA1, and differences between seasons were within 100 m. This pattern was captured by models. Similar as EA1, the simulated PBLH in EA2 was 100-200m higher than measurements. Few measurements on remote oceanic site were conducted in East Asia. So, we compared simulations with European Centre for Medium-Range Weather Forecasts Reanalysis Data (von Engeln et al., 2013). Both showed a winter-maximum pattern of PBLH.

The East Asia monsoon played an important role in seasonal cycle of O_3 in subregions by the long-range transport. Besides local intensive photochemical productions, the O_3 summer maxima in EA1were also affected by regional transport from Yangtze River Delta under prevailed summer southern monsoon (~20%) (Li et al., 2016). In EA2, a late maximum of O_3 in September-November was quite different from EA1 and EA3. This is largely attributed to the long-range transport of O_3 and its precursors in the polluted continental air masses from northern China and photochemical formation under dry and sunny weather conditions in autumn (Zheng et al., 2010). In EA3, the seasonal change of O_3 concentrations was characterized by two peaks in spring and autumn. The first and second peak in Mar–Apr and May and June were mainly influenced by the inflow from outside of East Asia and chemically produced O_3 by regional emissions, respectively. In the next studies, we will conduct the intermodel comparison on transport fluxes of O_3 between sub-regions over East Asia.

6. Summary

In the MICS-Asia III framework, the evaluation and intercomparison of 13 CTMs were conducted with a wide variety of observations covering two Chinese industrialized regions and western Pacific, using long-term simulations for the year 2010. This study has focused on O_3 , NO and NO_2. In particular, surface O_3 in China was evaluated, which was absent in the previous model-intercomparison projects. Large intermodel variability of O_3 existed in all subregions over East Asia in this study, with model concentrations varying by a factor of 2 to 3 between different models.

A model ensemble was conducted and evaluated. In general, the model ensemble captured the key pattern of monthly and diurnal O_3 ,NO and NO_2 in the North China Plain and the western Pacific Rim. It failed to capture the observed seasonal cycle of O_3 in Pearl River Delta of China. In North China Plain and western Pacific rim. The model ensemble severely overestimated surface O_3 in May-September by 10-30 ppbv. This overestimation systematically appeared in both daytime and nighttime. Similarly, the model ensemble had a predominate tendency to overestimate the daytime and nighttime O_3 concentrations in spring in Peral River Delta. Compared to MICS-Asia II, MICS-Asia III was less prone to underestimation of surface O_3 in March at Japanese sites. However, it predicted too enhanced surface O_3 concentrations at western Japan in July, which was not the case in MICS-Asia II. In term of O_3 soundings, the ensemble model in this study reproduced the vertical structure in western Pacific, but overestimated O_3 below 800 hpa in summer. In industrialized Pearl River Delta, the ensemble average presented an overestimation for O_3 in the lower troposphere and underestimation in the middle troposphere. This study revealed that ensemble average of 13 models on O_3 did not always exhibit a superior performance to certain individual models in East Asia, which contrasted with its performance in Europe. This suggested that the spread of ensemble-model values had not represented all uncertainties of O_3 or most models in MICS-Asia III missed key processes. Unlike the performance level for O_3, ENSE demonstrated superior performance level than individual models for NO_2 in East Asia.

MICS-Asia II guessed some potential reasons of variabilities among models. Quantifying the contribution of these processes to O_3 concentrations is one effective way to explain model biases by sensitivity simulations. But this required a tremendous amount of computational cost for 14 models. In this study, we conducted a qualitative analysis on potential causes by comparison between models and

observations on these processes to narrow sensitivity simulating scenarios for next phase of MICS-Asia. The comparison revealed that the ensemble model underestimated observed dry deposition velocities of O_3 in August-September in North China Plain, which could contribute to the overestimation of O_3 concentrations in summer. In western Pacific, simulated v_d agreed with observations reasonably. Photochemical treatment in models may contributed to the O_3 overestimation in North China Plain. Models captured the major pattern of climatology of PBLH observations in three subregions over East Asia. More evaluation on turbulent kinetic energy in PBL is urgent for assess the vertical mixing in future studies.

Author contribution：

JL, ZW and GC conducted the study design. JL, TN, BG, KY, JF, XW, QF, SI, HL, CK, CL, MZ, ZT, MK, HL contributed to modeling data. ML, JW, JK and QW provided the emission data. LK helped with data processing. HA, GC and ZW were involved in the scientific interpretation and discussion. JL prepared the manuscript with contributions from all co-authors.

Competing interests:

The authors declare that they have no conflict of interest.

Acknowledgements:

This work was supported by the Natural Science Foundation of China (41620104008; 41571130034; 91544227; 91744203), and National Key R&D Program of China (2017YFC0212402). This work was partly supported by the Environment Research and Technology Development Fund (S-12) of the Environmental Restoration and Conservation Agency of Japan and the Ministry of Environment, Japan. We thank the Pearl River Delta Regional Air Quality Monitoring Network for observations in Pearl River Delta. Dr. Kengo Sudo from Nagoya university and Prof. Rokjin J. Park provided us CHASER and GEOS-Chem outputs for boundary conditions. This manuscript was edited by Wallace Academic Editing.

Appendix A. Statistical Measures

Defining y_i and Obs_i modeled and observed concentrations of air pollutants at the i^{th} station, having mean value $\bar{y}$ and $\overline{obs}$

Correlation coefficient (R)

$$R = \frac{\sum_{i=1}^{n}(y_i-\bar{y})(obs_i-\overline{obs})}{\sum_{i=1}^{n}(y_i-\bar{y})^2 \sum_{i=1}^{n}((Obs_i-\overline{obs})^2} \quad (A1)$$

Root mean square error (RMSE):

$$\mathrm{RMSE} = \sqrt{\frac{\sum_i^n (y_i - Obs_i)^2}{n}} \qquad \text{(A2)}$$

Normalized Mean Bias (NMB)

$$\mathrm{NMB} = \frac{\sum_{i=1}^n (y_i - Obs_i)}{n \times \bar{y} \times \overline{Obs}} \qquad \text{(A3)}$$

References:

Ackermann, I. J., Hass, H., Memmesheimer, M., Ebel, A., Binkowski, F.S., and Shankar, U.: Modal aerosol dynamics model for Europe: Development and first applications, *Atmos. Environ.*, 32, No.17, 2981-2999,1998.

Akimoto, H., Mori, Y., Sasaki, K., Nakanishi, H., Ohizumi, T., Itano, Y.: Analysis of monitoring data of ground-level ozone in japan for long-term trend during 1990–2010: causes of temporal and spatial variation. *Atmos. Environ*., 102(9), 302-310,2015.

Akimoto, H., Nagashima, T., Li, J., Fu, J. S., Ji, D., Tan, J., and Wang, Z.: Comparison of surface ozone simulation among selected regional models in MICS-Asia III-effects of chemistry and vertical transport for the causes of difference, *Atmos. Chem. Phys*., 19, 603-615, https://doi.org/10.5194/acp-19-603-2019, 2019.

Ban, S., Matsuda, K., Sato, K., Ohizumi, T.: Long-term assessment of nitrogen deposition at remote EANET sites in Japan. *Atmos. Environ*., 146, 70-78,2016.

Banks, R. F., & Baldasano, J. M.: Impact of wrf model pbl schemes on air quality simulations over catalonia, spain. *Sci. Total Environ*, 572, 98-113,2016.

Binkowski, F.S. and Roselle, S. J.: Models 3-Community Multiscale Air Quality (CMAQ) model aerosol component:1. Model description, *J. Geophys. Res.-Atmos.*, 108(D6), 4183, doi:10.1029/2001JD001409, 2003.

Byun, D.W., Dennis, R.: Design artifacts in Eulerian air-quality models e evaluation of the effects of layer thickness and vertical profile correction on surface ozone concentrations. *Atmos. Environ*., 29, 105-126,1995.

Carlton, A. G., Turpin, B. J., Altieri, K. E., Seitzinger, S., Reff, A., Lim, H.-J., and Ervens, B.: Atmospheric oxalic acid and SOA production from glyoxal: Results of aqueous photooxidation experiment, *Atmos. Environ.*, 41, 7588–7602, 2007.

Carmichael, G. R., Calori, G., Hayami, H., Uno, I., Cho, S. Y., Engardt, M., Kim, S. B., Ichikawa, Y., Ikeda, Y., Woo, J. H., Ueda, H., Amann, M.: The MICS-Asia study: model intercomparison of long-range transport and sulfur deposition in East Asia， *Atmos. Environ*., 36, 175-199,2002.

Carmichael, G. R., Sakurai, T., Streets, D., Hozumi, Y., Ueda, H., Park, S.U., Fung, C., Han, Z., Kajino, M., Engardt, M., Bennet, C., Hayami, H., Sartelet, K., Holloway, T., Wang, Z., Kannari, A., Fu, J., Matsuda, K., Thongboonchoo, N., Amann, M., MICS-Asia II: The model intercomparison study for Asia Phase II methodology and overview of findings, *Atmos. Environ*, 42(15), 3468-3490, 2008.

Carter, W. P. L.: Implementation of the SAPRC-99 Chemical Mechanism into the Models-3 Framework, Report to the United States Environmental Protection Agency, available at: http://www.engr.ucr.edu/~carter/pubs/s99mod3.pdf (last access: 6 February 2015), 2000.

Colella, P., and Woodward, P. L.: The piecewise parabolic method (PPM) for gas-dynamical simulations, *J. Comput. Phys.*, 54, 174–201,1984

Easter, R. C., Ghan, S. J., Zhang, Y., Saylor, R. D., Chapman, E. G., Laulainen, N. S., Abdul-Razzak, H., Leung, L. R., Bian, X. D., and Zaveri, R. A.: MIRAGE: Model description and evaluation of aerosols and trace gases, J. Geophys. Res.-Atmos., 109, 46, 10.1029/2004jd004571, 2004.

Fiore, A. M., Dentener, F. J., Wild, O., Cuvelier, C., Schultz, M. G., Hess, P., Textor, C., Schulz, M., Doherty, R. M., Horowitz, L. W., MacKenzie, I. A., Sanderson, M. G., Shindell, D. T., Stevenson, D. S., Szopa, S., van Dingenen, R., Zeng, G., Atherton, C. S., Bergmann, D. J., Bey, I., Carmichael, G. R., Collins, W. J., Duncan, B. N., Faluvegi, G., Folberth, G. A., Gauss, M., Gong, S., Hauglustaine, D., Holloway, T., Isaksen, I. S. A., Jacob, D. J., Jonson, J. E., Kaminski, J. W., Keating, T. J., Lupu, A., Marmer, E., Montanaro, V., Park, R. J., Pitari, G., Pringle, K. J., Pyle, J. A., Schroeder, S., Vivanco, M. G., Wind, P., Wojcik, G., Wu, S., and Zuber, A.: Multimodel estimates of intercontinental source-receptor relationships for ozone pollution, *J. Geophys. Res.-Atmos*., 114(D4), 83-84, 2009.

Fountoukis, C. and Nenes, A.: ISORROPIA II: A Computationally Efficient Aerosol Thermodynamic Equilibrium Model for K^+, Ca^{2+}, Mg^{2+}, NH_4^+, Na^+, SO_4^{2-}, NO_3^-, Cl^-, H_2O Aerosols, *Atmos. Chem. Phys.*, 7, 4639–4659, 2007.

Ganzeveld, L., Helmig, D., Fairall, C. W., Hare, J., and Pozzer, A.: Atmosphere-ocean ozone exchange: A global modeling study of biogeochemical, atmospheric, and waterside turbulence dependencies, *Global Biogeochem. Cy*., 23, GB4021, doi:10.1029/2008GB003301, 2009.

Gao, M., Han, Z., Liu, Z., Li, M., Xin, J., Tao, Z., Li, J., Kang, J.-E., Huang, K., Dong, X., Zhuang, B., Li, S., Ge, B., Wu, Q., Cheng, Y., Wang, Y., Lee, H.-J., Kim, C.-H., Fu, J. S., Wang, T., Chin, M., Woo, J.-H., Zhang, Q., Wang, Z., and Carmichael, G. R.: Air quality and climate change, Topic 3 of the Model Inter-Comparison Study for Asia Phase III (MICS-Asia III) – Part 1: Overview and model evaluation, *Atmos. Chem. Phys.*, 18, 4859-4884, https://doi.org/10.5194/acp-18-4859-2018, 2018.

Chin, M., Ginoux, P., Kinne, S., Torres, O., Holben, B., Duncan, B.N., Martin, R.V., Logan, J., Higurashi, A., Nakajima T.: Tropospheric aerosol optical thickness from the GOCART model and comparisons with satellite and sun photometer measurements, *J. Atmos. Phys.*, 59 , 461-483,2012.

Gipson, G. L.: The Initial Concentration and Boundary Condition Processors. In Science algorithms of the EPA Models-3 Community Multiscale Air Quality (CMAQ) Modeling System, US Environmental Protection Agency Report, EPA-600/R-99/030, 12-1–12-91, 1999.

Goliff, W. S., Stockwell, W. R., Lawson, C. V.: The regional atmospheric chemistry mechanism, version 2. *Atmos. Environ.*, 68(1),174-185, 2013.

Guo, J., Miao, Y., Zhang, Y., Liu, H., Li, Z., Zhang, W., He, J., Lou, M., Yan, Y., Bian, L., and Zhai, P.: The climatology of planetary boundary layer height in china derived from radiosonde and reanalysis data, *Atmos. Chem. Phys.*, 16(20), 13309-13319, 2016.

Gutenther, A. K., T.; Harley, P.; Wiedinmyer, C.; Palmer, P.I.; Geron, C.: Estimates of global terrestrial isoprene emissions using MEGAN (Model of Emissions of Gases and Aerosols 921 from Nature, *Atmos. Chem. Phys.*, 6, 3181-3210, 2006.

Han, Z., Sakurai, T., Ueda, H., Carmichael, G. R., Streets, D., Hayami, H., Wang, Z., Holloway, T., Engardtg, M., Hozumib, Y., Parkh, S.U., Kajinoi, M., Sarteletj, K., Fungk, C., Bennetg, C.,

Thongboonchooc, N., Tangc, Y., Changk, A., Matsudal, K., Amannm, M. : MICS-ASIA II: model intercomparison and evaluation of ozone and relevant species, *Atmos. Environ*., 42(15), 3491-3509,2008.

Hardacre, C., Wild, O., and Emberson, L.: An evaluation of ozone dry deposition in global scale chemistry climate models, *Atmos. Chem. Phys*., 15, 6419-6436, https://doi.org/10.5194/acp-15-6419-2015, 2015.

He, J., Zhang, Y., Wang, K., Chen, Y., Leung, L. R., Fan, J., Li, M., Zheng, B., Zhang, Q., Duan, F., He, K. B.: Multi-year application of WRF-CAM5 over East Asia-Part II: Interannual variability, trend analysis, and aerosol indirect effects, *Atmos. Environ.*, 165,122-142, 2017.

Helmig, D., Lang, E. K., Bariteau, L., Boylan, P., Fairall, C. W., Ganzeveld, L., Hare, J. E., Hueber, J., and Pallandt, M.: Atmosphere-ocean ozone fluxes during the TexAQS 2006, STRATUS 2006, GOMECC 2007, GasEx 2008, and AMMA 2008 cruises, *J. Geophys. Res*., 117, D04305, doi:10.1029/2011JD015955, 2012.

Hong, S. Y.: A new vertical diffusion package with an explicit treatment of entrainment processes. Monthly Weather Review, 134(9), 2318,2006.

Horowitz, L. W., Walters, S. M., Mauzerall, D. L., Emmons, L. K., Rasch, P. J., Granier, C., Tie, X., Lamarque, J.-F., Schultz, M. G., and Brasseur, G. P: A global simulation of tropospheric ozone and related tracers: description and evaluation of MOZART, version 2, *J. Geophys. Res*.-*Atmos.*, 108 (D24), 4784. http://dx.doi.org/10.1029/2002JD002853,2003.

Huang, X., Song, Y., Li, M., Li, J., Huo, Q., Cai, X., Zhu, T., Hu, M., and Zhang, H.: A high-resolution ammonia emission inventory in China, *Global Biogeochem. Cy*., 26, GB1030, doi:10.1029/2011GB004161, 2012.

Ji, D., Wang, Y., Wang, L., Chen, L., Hub, B., Tang, G., Xin, J., Song, T., Wen, T., Sun, Y., Pan, Y., and Liu, Z.: Analysis of heavy pollution episodes in selected cities of northern China. *Atmos. Environ*. 50, 338-348, 2012.

Jin, X., Holloway, T.: Spatial and temporal variability of ozone sensitivity over China observed from the Ozone Monitoring Instrument, *J. Geophys. Res*.-*Atmos.*, 120(14),7229-7246,2015.

Kajino, M., Inomata, Y., Sato, K., Ueda, H., Han, Z., An, J., Katata, G., Deushi, M., Maki, T., Oshima, N., Kurokawa, J., Ohara, T., Takami, A., and Hatakeyama, S.: Development of the RAQM2 aerosol chemical transport model and predictions of the Northeast Asian aerosol mass, size, chemistry, and mixing type, *Atmos. Chem. Phys.*, 12, 11833-11856, https://doi.org/10.5194/acp-12-11833-2012, 2012.

Kajino, M., Deushi, M., Sekiyama, T. T., Oshima, N., Yumimoto, K., Tanaka, T. Y., Ching, J., Hashimoto, A., Yamamoto, T., Ikegami, M., Kamada, A., Miyashita, M., Inomata, Y., Shima, S., Adachi, K., Zaizen, Y., Igarashi, Y., Ueda, H., Maki, T., and Mikami, M.: NHM-Chem, the Japan Meteorological Agency's regional meteorology - chemistry model (v1.0): model description and aerosol representations, *Geosci. Model Dev. Discuss*, in review, doi:10.5194/gmd-2018-128, 2018.

Kurokawa, J., Ohara, T., Morikawa, T., Hanayama, S., Janssens-Maenhout, G., Fukui, T., Kawashima, K., and Akimoto, H.: Emissions of air pollutants and greenhouse gases over Asian regions during 2000–2008: Regional Emission inventory in ASia (REAS) version 2, *Atmos. Chem. Phys.*, 13, 11019-11058, doi:10.5194/acp-13-11019-2013, 2013.

Lee, D. G., Lee, Y.M., Jang, K.W., Yoo, C., Kang, K.H., Lee, J.H., Jung, S.W., Park, J.M., Lee, S.B., Han, J.S., Hong, J.H., and Lee, S.J.: Korean national emissions inventory system and 2007 air pollutant emissions, *Asian J. Atmos. Environ.*, 5, 278-291, 2011.

Lelieveld, J. and Dentener, F. J.: What controls tropospheric ozone?, *J. Geophys. Res.*, 105, 3531–3551, doi:10.1029/1999JD901011, 2000

Li, J., Chen, X., Wang, Z., Du, H., Yang, W., Sun, Y., Hu, B., Li, J. J., Wang, W., Wang, T., Fu, P., Huang, H.: Radiative and heterogeneous chemical effects of aerosols on ozone and inorganic aerosols over East Asia, *Sci. Total Environ.*, 622-623,1327-1342, 2018.

Li, J., Wang, Z., Akimoto, H., Gao, C., Pochanart, P., and Wang, X.: Modeling study of ozone seasonal cycle in lower troposphere over East Asia, *J. Geophys. Res.-Atmos.*, 112, D22S25, doi:10.1029/2006JD008209, 2007.

Li, J., Wang, Z., Akimoto, H., Tang, J., Uno, I.: Near-ground ozone source attributions and outflow in central eastern China during MTX2006 *Atmos. Chem. Phys.*, 8, 7335-7351,2008.

Li, J., Yang, W., Wang, Z., Chen, H., Hu, B., Li, J., Sun, Y., Fu, P., Zhang, Y.: Modeling study of surface ozone source-receptor relationships in east Asia. *Atmos. Res.*, 167, 77-88, 2016.

Li, M., Zhang, Q., Kurokawa, J. I., Woo, J. H., He, K., Lu, Z., Ohara, T., Song, Y., Streets, D. G., Carmichael, G. R., Cheng, Y., Hong, C., Huo, H., Jiang, X., Kang, S., Liu, F., Su, H., and Zheng, B.: MIX: a mosaic Asian anthropogenic emission inventory under the international collaboration framework of the MICS-Asia and HTAP, *Atmos. Chem. Phys*., 17, 935-963, doi:10.5194/acp-17-935-2017, 2017.

Li, M., Zhang, Q., Kurokawa, J., Woo, J.H., He, K.B., Lu, Z., Ohara, T., Song, Y., Streets, D.G., Carmichael, G.R., Cheng, Y.F., Hong, C.P., Huo, H., Jiang, X.J., Kang, S.C., Liu, F., Su, H., Zheng, B.: MIX: a mosaic Asian anthropogenic emission inventory for the MICS-Asia and the HTAP projects. *Atmos. Chem. Phys. Discuss*. 15 (23), 34813-34869. http://dx.doi.org/10.5194/acpd-15-34813-2015,2015.

Loon, M., Vautard, R., Schaap, M., Bergstr, M, R., Bessagnet, B., Brandt, J., Builtjes, P.J.H., Christensen, J. H., Curvelier, C., Graff, A., Jonson, J. E., Krol, M., Langner, J., Roberts, P., Rouil, L.M., Stern, R., Tarrason, L., Thunis, P., Vignati, E., White, L., Wind, P.: Evaluation of long-term ozone simulations from seven regional air quality models and their ensemble. *Atmos. Environ*., 41(10), 2083-2097,2007.

Lin, J. T., & Mcelroy, M. B. : Impacts of boundary layer mixing on pollutant vertical profiles in the lower troposphere: implications to satellite remote sensing. *Atmos. Environ.*, 44(14), 1726-1739, 2010.

Liu, S. C., McKeen, S. A., Hsie, E-Y., Lin, X., Kelly, K. K., Bradshaw, J. D., Sandholm, S. T., Browell, E. V., Gregory, G. L., Sachse, G. W., Bandy, A. R., Thornton, D. C., Blake, D. R., Rowland, F. S., Newell, R., Heikes, B. G., Singh, H., and Talbot, R. W. : Model study of tropospheric trace species distributions during PEM-West A, J. Geophys. Res., 101, 2073-2085,1996.

Liu, X. H., Zhang, Y., Xing, J., Zhang, Q., Wang, K., Streets, D. G., Jang, C., Wang, W. X., Hao, J. M.: Understanding of regional air pollution over China using CMAQ, part II. Process analysis and sensitivity of ozone and particulate matter to precursor emissions, *Atmos. Environ*. 44, 3719-3727, 2010.

Lu, Z., and Streets, D. G.: Increase in NO_x Emissions from Indian Thermal Power Plants during 1996-2010: Unit-Based Inventories and Multisatellite Observations, *Environ. Sci. Technol*., 46, 7463-7470, doi:10.1021/es300831w, 2012.

Lu, Z., Zhang, Q., and Streets, D. G.: Sulfur dioxide and primary carbonaceous aerosol emissions in China and India, 1996-2010, *Atmos. Chem. Phys*., 11, 9839-9864, doi:10.5194/acp-11-9839-2011, 2011.

Martin, R. V., Jacob, D. J., Logan, J. A., Bey, I., Yantosca, R. M., Staudt, A. C., Li, Q., Fiore, A. M., Duncan, B. N., and Liu, H.: Interpretation of TOMs observations of tropical tropospheric ozone with a global model and in situ observations, *J. Geophys. Res*.-*Atmos*, 107(D18), ACH 4-1–ACH 4-27, 2002.

Nagashima, T., Ohara, T., Sudo, K., and Akimoto, H.: The relative importance of various source regions on East Asian surface ozone, *Atmos. Chem. Phys*., 10, 11305-11322, https://doi.org/10.5194/acp-10-11305-2010, 2010.

Nenes, A., Pandis, S.N., Pilinis, C. : ISORROPIA: A new thermodynamic equilibrium model for multiphase multicomponent inorganic aerosols, *Aquat. Geoch*., 4, 123-152,1998.

Olson, J., Prather, M., Berntsen, T., Carmichael, G., Chatfield, R., Connell, P., Derwent, R., Horowitz, L., Jin, S., Kanakidou, M., Kasibhatla, P., Kotamarthi, R., Kuhn, M., Law, K., Penner, J., Perliski, L., Sillman, S., Stordal, F., Thompson, A., and Wild, O.: Results from the intergovernmental panel on climatic change photochemical model intercomparison(PhotoComp), *J. Geophys. Res*.-*Atmos.*, 102 (D5),5979–5991,1997.

Pan, X., Wang Z., Wang X., Dong H., Xie, F., Guo, Y.: An observation study of ozone dry deposition over grassland in the suburban area of Beijing. Chinese Journal of Atmospheric Sciences (in Chinese), 34(1), 120-130, 2010.

Pleim, J. E., Xiu, A., Finkelstein, P. L., and Otte, T. L.: A Coupled Land-Surface and Dry Deposition Model and Comparison to Field Measurements of Surface Heat, Moisture, and Ozone Fluxes, *Water Air Soil Poll.*, 1, 243–252, 2001.

Pleim, J. E.: A combined local and nonlocal closure model for the atmospheric boundary layer, Part I: Model description and testing, *J. Appl. Meteor. Climatol.*, 46, 1383–1395, 2007.

Quan, J., Tie, X., Zhang, Q., Liu, Q., Li, X., Gao, Y., and Zhao, D.: Evolution of planetary boundary layer under different weather conditions, and its impact on aerosol concentrations, Particuology, 11(1), 34-40, 2013.

Rao, S. T., Galmarini, S., Puckett, A. K.: Air quality model evaluation international initiative (AQMEII): advancing state-of-science in regional photochemical modeling and its applications, BAMS, 23-30, 2011.

Santanello, A., Lidard, C. D., Kennedy, A., Kumar, S.V.: Diagnosing the nature of land-atmosphere coupling: a case study of dry/wet extremes in the U.S. Southern Great Plains, *J. Hydrometeor*., 14, 3-24, 10.1175/JHM-D-12-023.1,2013.

Sillman, S., and He, D.: Some theoretical results concerning O_3-NO_x-VOC chemistry and NOx-VOC indicators, *J. Geophys. Res.-Atmos.*, 107(D22), 4659, doi:10.1029/2001JD001123, 2002.

Solazzo, E., Bianconi, R., Pirovano, G., Matthias, V., Vautard, R., Appel, K. W., Bessagnet, B., Brandt, J., Christensen, J. H., Chemel, C., Coll, I., Ferreira, J., Forkel, R., Francis, X. V., Grell, G., Grossi, P., Hansen, A., Miranda, A. I., Moran, M. D., Nopmongco, U., Parnk, M., Sartelet, K. N., Schaap, M., D. Silver, J., Sokhi, R. S., Vira, J., Werhahn, J., Wolke, R., Yarwood, G., Zhang, J., Rao, S. T., Galmarin, S.: Model evaluation and ensemble modelling of surface-level ozone in Europe and north America in the context of AQMEII, *Atmos. Environ*, 53(6), 60-74,2012.

Sorimachi, A, Sakamoto, K, Ishihara H, Fukuyama, T., Utiyama, M., Liu, H., Wang, W., Tang, D., Dong, X., Quan, H.: Measurements of sulfur dioxide and ozone dry deposition over short vegetation in northern China-A preliminary study. *Atmos. Environ.*, 37(22), 3157-3166, 2003.

Stockwell, W. R., Middleton, P., Chang, J. S. and Tang, X.: The second generation regional Acid Deposition Model chemical mechanism for regional air quality modeling, *J. Geophys. Res.*, 95, 16,343-16,367, 1990.

Streets, D. G., Fu, J. S., Jang, C. J., Hao, J. M., He, K. B., Tang, X. Y., Zhang, Y. H., Wang, Z. F., Li, Z. P., Zhang, Q., Wang, L. T., Wang, B. Y., and Yu, C: Air quality during the 2008 Beijing Olympic games，*Atmos. Environ*, 41(3), 480-492, 2007.

Sudo, K., Takahashi, M., Kurokawa, J. I., Akimoto, H.: Chaser: a global chemical model of the troposphere 1. model description. *J. Geophys. Res.-Atmos.*, 107(D17), ACH 7-1–ACH 7-20., 2002a.

Sudo, K., Takahashi, M., Akimoto, H., CHASER: A global chemical model of the troposphere 2. Model results and evaluation, *J. Geophys. Res.*, 107, 10.1029/2001/JD001114, 2002b.

Tang, H., Takigawa, M., Liu, G. , Zhu, J., Kobayashi, K.: A projection of ozone induced wheat production loss in China and India for the years 2000 and 2020 with exposure-based and flux-based approaches, *Glob. Change Biol.*, 19, 2739-2752, 2013.

Tang, X, Wang, Z., Zhu, J., Abaguidi, A., Wu, Q., Li, J., Zhu, T.: Sensitivity of ozone to precursor emissions in urban Beijing with a Monte Carlo scheme. *Atmos. Environ.*, 44(31),3833-3842, 2010.

Tao, Z., Santanello, J. A., Chin, M., Zhou, S., Tan, Q., Kemp, E. M., and Peters-Lidard, C. D.: Effect of land cover on atmospheric processes and air quality over the continental United States – a NASA Unified WRF (NU-WRF) model study, *Atmos. Chem. Phys*., 13, 6207-6226, https://doi.org/10.5194/acp-13-6207-2013, 2013.

The Royal Society: Ground-level ozone in the 21st century: future trends, impacts and policy implications, Policy Document, 15/08,2008.

von Engeln, A. V. and Teixeira, J. A.: Planetary boundary layer height climatology derived from ECMWF reanalysis Data, *J. Clim*., 26(17), 6575-6590, 2013.

Walcek, C. J. and Aleksic, N. M.: A simple but accurate mass conservative peak-preserving, mixing ratio bounded advection algorithm with fortran code, *Atmos. Environ.*, 32, 3863–3880, 1998

Walcek, C. J. and Teylor, G. R.: A theoretical method for computing vertical distributions of acidity and sulfate production within cumulus clouds, *J. Atmos. Sci.*, 43, 339–355, 1986.

Wang, S., Ackermann, R., and Stutz, J.: Vertical profiles of O_3 and NO_x chemistry in the polluted nocturnal boundary layer in Phoenix, AZ: I. Field observations by long-path DOAS, *Atmos. Chem. Phys.*, 6, 2671-2693, https://doi.org/10.5194/acp-6-2671-2006, 2006.

Wang, W. N., Cheng, T. H., Gu, X. F., Chen, H., Guo, H., Wang, Y., Bao, F. W., Shi, S. Y., Xu, B. R., Zuo, X., Meng, C., Zhang, X. C.. Assessing spatial and temporal patterns of observed ground-level ozone in China. Scientific Reports, 7(1), 3651. doi:10.1038/s41598-017-03929-w, 2007.

Wang, Y. X., Shen, L. L., Wu, S., Mickley, L., He, J. W., Hao, J.: Sensitivity of surface ozone over China to 2000–2050 global changes of climate and emissions, *Atmos. Environ*, 75, 374-382, 2013.

Wesely, M. L.: Parameterization of surface resistances to gaseous dry deposition in regional-scale numerical models, *Atmos. Environ*, 23(6), 1293-1304,1989.

World Health Organization (WMO), WHO air quality guidelines global update, report on a working group meeting. Born, Germany,18-20 October, 2005, *Rep*. ,25 pp., Geneva, 2005.

Yamaji, K., Ohara, T., Uno, I., Tanimoto, H., Kurokawa, J. I., Akimoto, H.: Analysis of the seasonal variation of ozone in the boundary layer in east Asia using the community multi-scale air quality model: what controls surface ozone levels over Japan?, *Atmos. Environ*, 40(10), 1856-1868, 2006.

Yamartino, R. J.: Nonnegative, conserved scalar transport using grid-cell-centered, spectrally constrained Blackman cubics for applications on a variable-thickness mesh, *Mon. Weather Rev*., 121, 753–763, 1993

Yarwood, G., Rao, S., Yocke, M., Whitten, G.: Updates to the Carbon Bond Chemical Mechanism: CB05 Final Report to the US EPA, RT-0400675,2005.

Zaveri, R, A,, Peters, L. K.: A new lumped structure photochemical mechanism for large-scale applications. *J. Geophys. Res*.104, 30387-30415,1999.

Zhang, J., Trivikrama, Rao, S.: The role of vertical mixing in the temporal evolution of ground-level ozone concentrations, *J. Appl. Meteo*., 38(38), 1674-1691,1998.

Zhang, L., Brook, J. L., and Vet, R.: A revised parameterization for gaseous dry deposition in air-quality models, *Atmos. Chem. Phys*., 3, 2067-2082, 2003.

Zhang, Y.H., Hu, M., Zhong, L. J. , Wiedensohler, A., Liu, S.C., Andreae, M.O., Wang, W. , Fan, S. J.: Regional Integrated Experiments on Air Quality over Pearl River Delta 2004 (PRIDE-PRD2004): Overview, *Atmos. Environ*, 42(25), 6157-6173, 2008.

Zhao, C., Wang, Y., Zeng. T.: East China Plains: a "Basin" of ozone pollution, *Environ. Sci. Technol*., 43, 1911-1915, 2009.

Zhong, L., Louie, P. K., Zheng, J., Wai, K. M., Ho, J. W. K., Yuan, Z., Lau A. K. H., Yue D. L., Zhou Y.: The pearl river delta regional air quality monitoring network - regional collaborative efforts on joint air quality management. *Aero. Air Qual. Res.*, 13(5), 1582-1597, 2013.

Table and Figure captions:

Table.1 Basic structures, schemes and relevant parameters of the fourteen participating models

Table. 2 Statistical analysis for surface O_3 in three subregions over East Asia (R: correlation coefficient; NMB: Normalized Mean Bias; RMSE: Root Mean Square Error)

Table. 3 Statistical analysis for surface NO in three subregions over East Asia (R: correlation coefficient; NMB: Normalized Mean Bias; RMSE: Root Mean Square Error)

Table. 4 Statistical analysis for surface NO_2 in three subregions over East Asia (R: correlation coefficient; NMB: Normalized Mean Bias; RMSE: Root Mean Square Error)

Fig. 1 Model domain of models except M13 and M14 with locations of three sub-regions marked in this study. Also show are locations of surface monitoring stations in this study. The meteorological model used for providing meteorological fields with most models also use this domain. Note that the domains of M13 and M14 are shown in Fig.10.

Fig. 2 Box-plots of observed and simulated annual NO_2 (left column), NO (middle column) and O_3 (right column) frequency distribution by 13 models, averaged in stations over EA1, EA2 and EA3, and in time for the whole 2010 year. n represents the numbers of stations. The rectangle represents the inter-quantile range (25^{th} to 75^{th} percentile). The small star identifies the mean, the continuous horizontal line inside the rectangle identifies the median, the whiskers extend between the minimum and maximum values.

Fig. 3 Time series of monthly NO_2, NO and O_3 simulated by all models and their ensembles (Ense), in ppbv, averaged over all observed stations in three subregions over East Asia (EA1: top row, EA2: middle row, EA3: bottom row). Observations are also shown by the black line. n represents the numbers of stations

Fig. 4 Seasonal mean diurnal cycle of surface O_3, in ppbv, as a function of hour, for all models and their ensembles, averaged over all observed stations in three subregions over East Asia (EA1: top row, EA2: middle row, EA3: bottom row). Observations are also shown by the black line. n represents the numbers of stations

Fig. 5 Simulated O_3 profiles in summer and winter of 2010, averaged over all observed stations in three subregions over East Asia (EA1: left column, EA2: middle column, EA3: bottom column). The ozonesonde data observe in 2010 was taken from the data base stored by World Ozone and Ultraviolet Radiation Data Centre (WOUDC)

Fig. 6 The ensemble mean seasonal surface O_3 concentrations and CV for the different seasons. CV is defined as the standard deviation of the modeled fields divided by the average, for the different seasons

Fig. 7 Surface O_3 spatial distribution from 13 models for summer 2010 (unit: ppbv).

Fig. 8 The modeled and observed monthly mean concentrations of O_3 at EANET sites in the phase II (left panel) and III (right panel) of MICS-ASIA project. Solid line represents ensemble mean. Note that data in MCIS-ASIA II and III are in the period of March, July and December of 2001 and 2010, respectively. ID of Monitoring sites represents: 1: Rishiri (45.12°N, 141.23°E), 2:Ogasawara (27.83°N, 142.22°E), 3: Sado-seki (38.23°N, 138.4°E), 4: Oki (36.28°N, 133.18°E), 5: Hedo (26.85°N,128.25°E), 6：Banryu (34.67°N,131.80°E)

Fig. 9 Simulated and observed monthly O_3 dry deposition velocities (V_d) of M1, M2, M4, M6, M11, M12, M13 and M14 in three subregions over East Asia (EA1: top row, EA3: middle row, EA3: bottom row). TEX, STR, GGSEX and AMMA represents observations in TexAQS06 (7 July–12 September 2006; north-western Gulf of Mexico), STRATUS06 (9–27 October 2006; the persistent stratus cloud region off Chile in the eastern Pacific Ocean), GasEx08 (29 February– 11 April 2008; the Southern Ocean), and AMMA08 (27 April–18 May 2008; the southern and northern Atlantic Ocean). Observation data is from Sorimachi et al. (2003), Pan et al. (2010), and Helmig et al. (2012).

Fig. 10 Scatter plots between monthly daytime (08:00-20:00) surface NO_x and O_3 at each station over EA1 (red), EA2 (green)and EA3 (blue) in May-October, for observations (obs) and models. Also shown are the linear regression equations between NO_x and O_3 in EA1 (red) and EA2 (green).

Table1 Basic structures, schemes and relevant parameters of the fourteen participating models

Models	M1	M2	M3	M4	M5	M6	M7	M8	M9	M10	M11	M12	M13	M14
Domain	Ref[a]	Ref[a]	Ref[a]	Ref[a]	Ref[a]	Ref[a]	Ref[a]	Ref[a]	Ref[a]	Ref[a]	Ref[a]	Ref[a]	Global	10 °N -50°N; 80 °E -135 °E
Horizontal resolution	45km	45km	45km	45km	45km	45km	45km	45km	45km	45km	45km	45km	0.5 ° ×0.667°	45km
Vertical resolution	40σ_p levels	40σ_p levels	40σ_p levels	40σ_p levels	40σ_p levels	40σ_p levels	40σ_p levels	40σ_p levels	40σ_p levels	60σ_p levels	20σ_z levels	40σ_p levels	47σ_p levels	15σ_z levels
Depth of first layer	58m	58m	58m	58m	58m	58m	29m	58m	16m	44m	48m	27m		100m
Meteorology	Standard[b]	Standard[b]	Standard[b]	Standard[b]	Standard[b]	Standard[b]	WRF/NCEP[b]	WRF/NCEP[b]	WRF/NCEP[b]	WRF/ MERRA2[b]	Standard[b]	Standard[b]	GEOS-5	RAMS/NCEP[b]
Advection	Yamo (Yamartino, 1993)	Yamo	Yamo	PPM(Colella and Woodward 1984)	PPM	Yamo	5th order monotonic	5th order monotonic	5th order monotonic	5th order monotonic	Walcek and Aleksic (1998)	Walcek and Aleksic (1998)	PPM	PPM
Vertical diffusion	ACM2 (Pleim,2007)	ACM2	ACM2	ACM2	ACM2	ACM2	3th order Monotonic	3th order Monotonic	YSU	YSU	K-theory	FTCS (Forward in Time, Center in Space)	Lin and McElroy, (2010)	ACM2
Dry deposition	Wesely (1989)	Wesely (1989)	Wesely (1989)	M3DRY (Pleim et al., 2001)	M3DRY	M3DRY	Wesely (1989)	Wesely (1989)	Wesely (1989)	Wesely (1989)	Wesely (1989)	Wesely(1989)and Zhang et al. (2003)	Wesely (1989)	Wesely（1989）

Wet deposition	Henry's Law	Henry's Law	Henry's Law	Henry's Law	Henry's Law	ACM	Henry's Law	AQCHEM	Easter et al., (2004)	Grell	Henry's Law	Henry's Law	Henry's Law	Henry's Law
Gas chemistry	SAPRC99(Carter,2 000)	SAPRC99	CBM05(Yarwood et al.,2005)	SAPRC99	SAPRC99	SAPRC99	RACM-ESRL with KPP	RACM (Goliff et al., 2013)	RADM2 (Stockwell et al., 1990)	RADM2	CBMZ (Zaveri et al.,1999)	SAPRC99(Carter,2000)	NOx-Ox-HC chemistry mechanism	SAPRC99
Aqueous chemistry	ACM-ae6	ACM-ae6	ACM-ae5	ACM-ae5	ACM-ae5	ACM-ae5	CMAQ simplified Aqueous chemistry	AQCHEM	Walcek and Taylor (1986)	None	RADM2 (Stockwell et al., 1990)	Walcek and Teylor (1986) Carlton et al. (2007)	-	ACM
Inorganic mechanism	AER06(Binkowski and Roselle, 2003)	AER06	AER05	AER05	AER05	AER05	MADE (Ackermann et al., 1998)	MADE	MADE	GOCART	ISORROPIAv1.7(Nenes et al.,1998)	Kajino et al. (2012)	ISORROPIAv1.7	ISORROPIAv1.7
Boundary conditions	GEOS-Chem global model (Martin et al.,2002)	Gipson (1999)	GEOS-Chem global model	CHASER global model (Sudo et al., 2002a, 2002b)	CHASER global model	CHASER global model	Liu et al. (1996)	CHASER global model	GEOS-Chem global model	MOZART + GOCART global models[c]	CHASER global model	CHASER global model	/	GEOS-Chem global model
Two-way feedback	Off-line	Off-line	Off-line	Off-line	Off-line	Off-line	On-line	On-line	On-line	Off-line	Off-line	On-line	Off-line	Off-line

[a] Ref represent the referenced domain by MICS-ASIA III project.

[b]Standard represents the reference meteorological field provided by MICS-ASIAIII project; WRF/NCEP and WRF/MERRA represents the meteorological field of the participating model itself, which was run by WRF driven by the NCEP and Modern Era Retrospective-analysis for Research and Applications (MERRA) reanalysis dataset.

[c]Boundary conditions of M10 are from MOZART and GOCART (Chin et al., 2002; Horowitz et al.,2003), which provided results for gaseous pollutants and aerosols, respectively.

Table 2 Statistical analysis for surface O_3 in three subregions over East Asia (R: correlation coefficient; NMB: Normalized Mean Bias; RMSE: Root Mean Square Error, unit is ppbv)

Models	Region	R	NMB	RMSE	Region	R	NMB	RMSE	Region	R	NMB	RMSE
M1		0.89	0.52	19.79		0.48	0.31	14.41		0.57	0.28	15.49
M2		0.90	0.64	18.13		0.10	0.35	15.06		0.66	0.24	13.83
M4		0.87	0.44	18.78		0.41	0.36	14.15		0.01	0.05	17.57
M5		0.87	0.42	19.00		0.30	0.14	13.38		0.34	0.31	19.28
M6		0.90	0.88	25.41		0.15	0.44	17.41		0.52	0.31	16.52
M7	EA1 (n=19)[a]	0.84	0.25	10.03	EA2 (n=13)	0.29	-0.08	11.11	EA3 (n=8)	0.60	0.02	10.97
M8		0.78	-0.47	13.52		0.20	-0.59	19.54		0.55	-0.27	15.32
M9		0.85	0.59	14.84		0.63	0.48	15.69		0.26	-0.09	13.27
M10		0.82	1.24	32.70		0.51	0.72	21.71		0.52	0.11	12.68
M11		0.81	0.09	9.46		0.34	-0.25	13.40		0.65	0.15	12.09
M12		0.89	0.55	18.53		0.36	0.30	13.31		0.57	0.11	11.81

M13	0.86	0.95	22.69	0.25	0.50	17.04	0.63	0.09	11.04
M14	0.86	0.75	23.33	0.12	0.40	17.01	-0.13	-0.30	20.03
Ensemble Mean	0.89	0.53	15.92	0.38	0.23	11.76	0.52	0.08	11.93
Ensemble Media	0.89	0.56	17.86	0.37	0.31	13.29	0.54	0.11	12.06

a: n represents the numbers of observation stations

Table 3 Statistical analysis for surface NO in three subregions over East Asia (R: correlation coefficient; NMB: Normalized Mean Bias; RMSE: Root Mean Square Error, unit is ppbv)

Models	Region	R	NMB	RMSE	Region	R	NMB	RMSE	Region	R	NMB	RMSE
M1		0.58	-0.35	20.68		0.22	-0.81	15.16		0.03	-0.35	0.23
M2		0.57	-0.14	23.73		0.14	-0.73	15.21		0.06	-0.27	0.19
M4		0.60	-0.61	22.29		0.18	-0.87	15.72		0.00	-0.39	0.20
M5		0.57	-0.07	20.34		0.24	-0.29	13.80		0.02	0.08	0.35
M6	EA1 (n=19)	0.60	-0.71	23.36	EA2 (n=13)	0.11	-0.89	15.94	EA3 (n=8)	0.15	-0.70	0.16
M7		0.63	-0.75	24.91		0.04	-0.78	15.32		0.27	-0.40	0.15
M8		0.65	0.91	26.89		0.29	1.14	25.06		0.24	3.53	0.94
M9		0.58	-0.82	27.73		0.32	-0.93	16.72		0.22	-0.54	0.14
M10		0.63	-0.90	27.97		0.27	-0.94	16.30		0.39	-0.51	0.14
M11		0.61	-0.34	19.92		0.04	-0.05	14.86		0.41	0.09	0.14

M12	0.62	-0.55	21.19	0.13	-0.85	15.64	0.17	-0.48	0.16
M13	-	-	-	-	-	-	-	-	-
M14	0.68	-0.66	22.74	0.01	-0.66	14.77	0.24	-0.50	0.15
Ensemble Mean	0.63	-0.42	20.12	0.21	-0.55	13.58	0.20	-0.03	0.19
Ensemble Media	0.62	-0.58	21.66	0.17	-0.83	15.40	0.17	-0.45	0.16

a: n represents the numbers of observation stations

Table 4 Statistical analysis for surface NO_2 in three subregions over East Asia (R: correlation coefficient; NMB: Normalized Mean Bias; RMSE: Root Mean Square Error, unit is ppbv)

Models	Region	R	NMB	RMSE	Region	R	NMB	RMSE	Region	R	NMB	RMSE
M1		0.59	-0.18	11.08		0.33	-0.30	12.92		0.54	0.27	1.51
M2		0.64	-0.25	11.30		0.25	-0.43	14.85		0.43	-0.07	1.13
M4		0.65	-0.28	11.62		0.26	-0.32	13.79		0.56	-0.07	1.04
M5		0.57	0.08	10.86		0.30	0.09	12.91		0.60	0.46	1.79
M6	EA1 (n=19)	0.65	-0.22	11.04	EA2 (n=13)	0.23	-0.30	13.86	EA3 (n=8)	0.56	-0.23	0.90
M7		0.59	-0.22	11.42		0.20	-0.25	13.24		0.65	0.19	1.42
M8		0.43	14.32	11.90		0.43	0.15	10.97		0.72	2.38	4.46
M9		0.60	32.30	18.80		0.51	-0.37	12.66		0.49	0.05	1.66
M10		0.61	-10.61	10.65		0.15	-0.08	12.81		0.63	0.06	1.33

M11	0.54	0.00	10.82	0.24	0.13	13.56	0.69	0.36	1.58
M12	0.63	-0.16	10.76	0.25	-0.24	13.78	0.61	-0.05	0.91
M13	-	-	-	-	-	-	-	-	-
M14	0.66	-0.12	10.00	0.08	-0.22	14.50	0.60	0.42	0.91
Ensemble Mean	0.65	-0.09	9.89	0.29	-0.18	12.16	0.64	0.25	1.33
Ensemble Media	0.65	-0.13	10.07	0.27	-0.23	12.85	0.59	0.06	1.23

a: n represents the numbers of observation stations

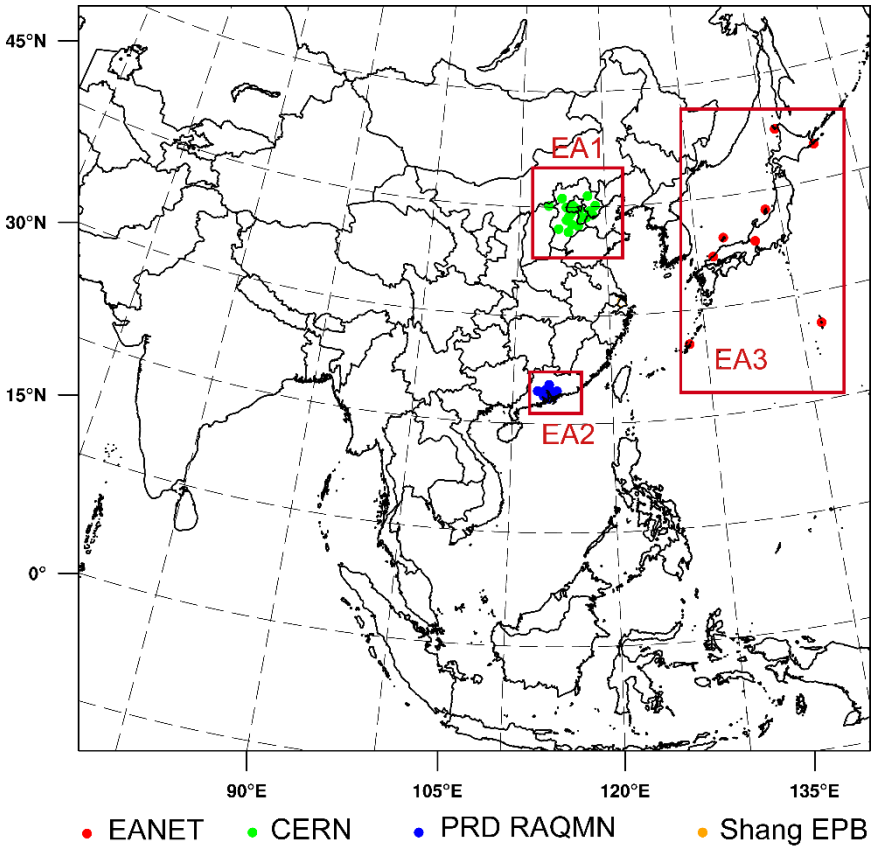

Fig.1 Li et al., 2018

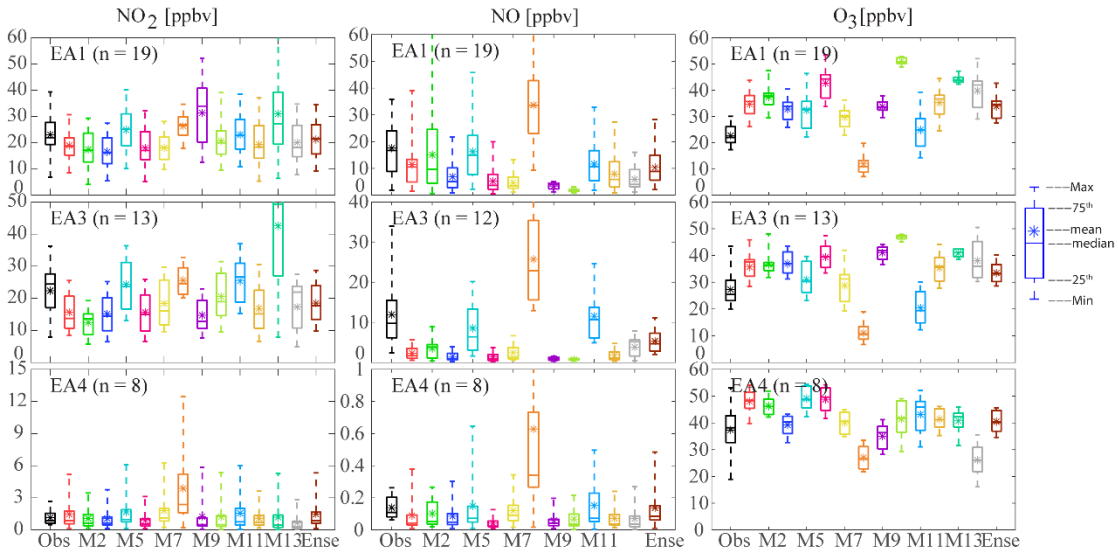

Fig.2 Li et al., 2018

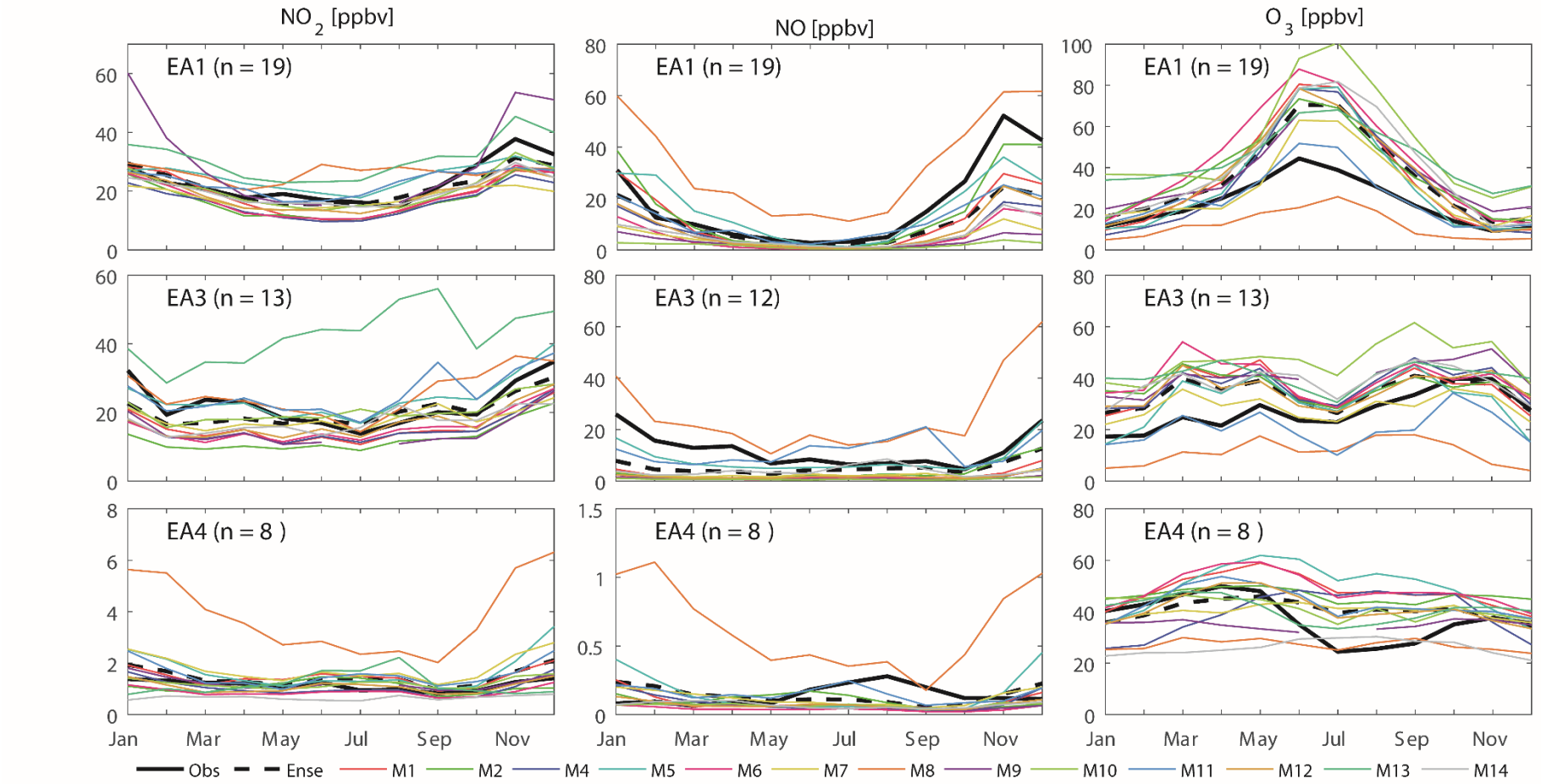

Fig.3 Li et al., 2018

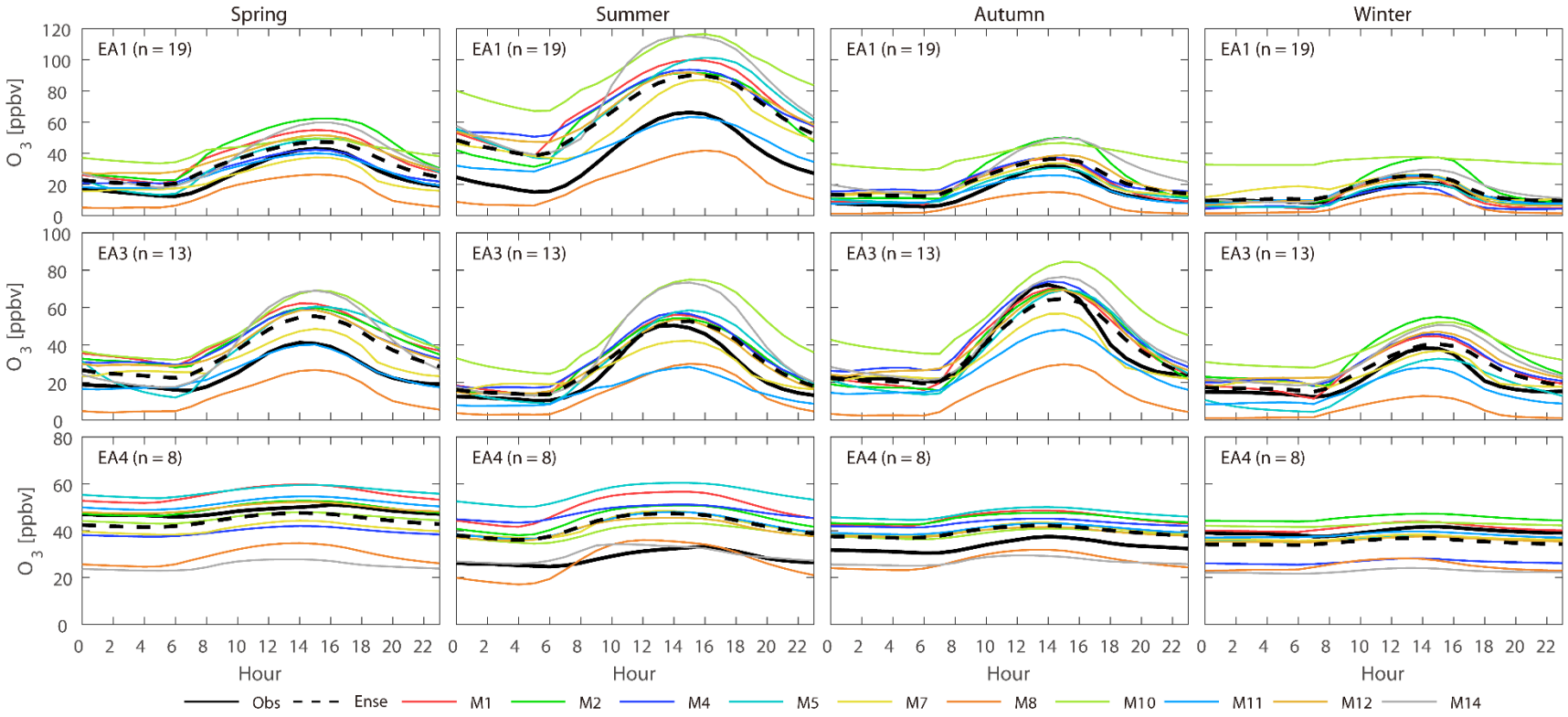

Fig.4 Li et al., 2018

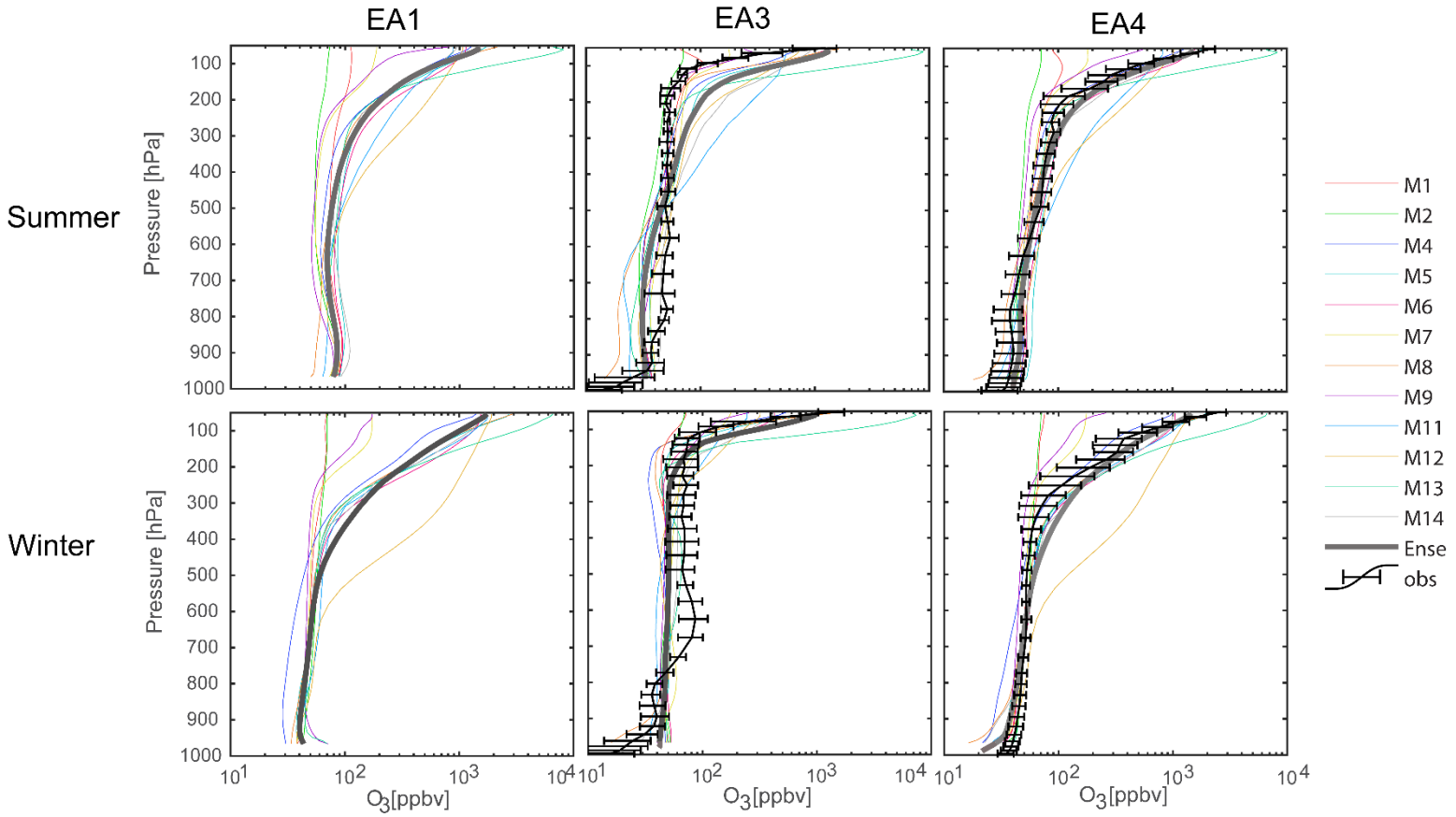

Fig.5 Li et al., 2018

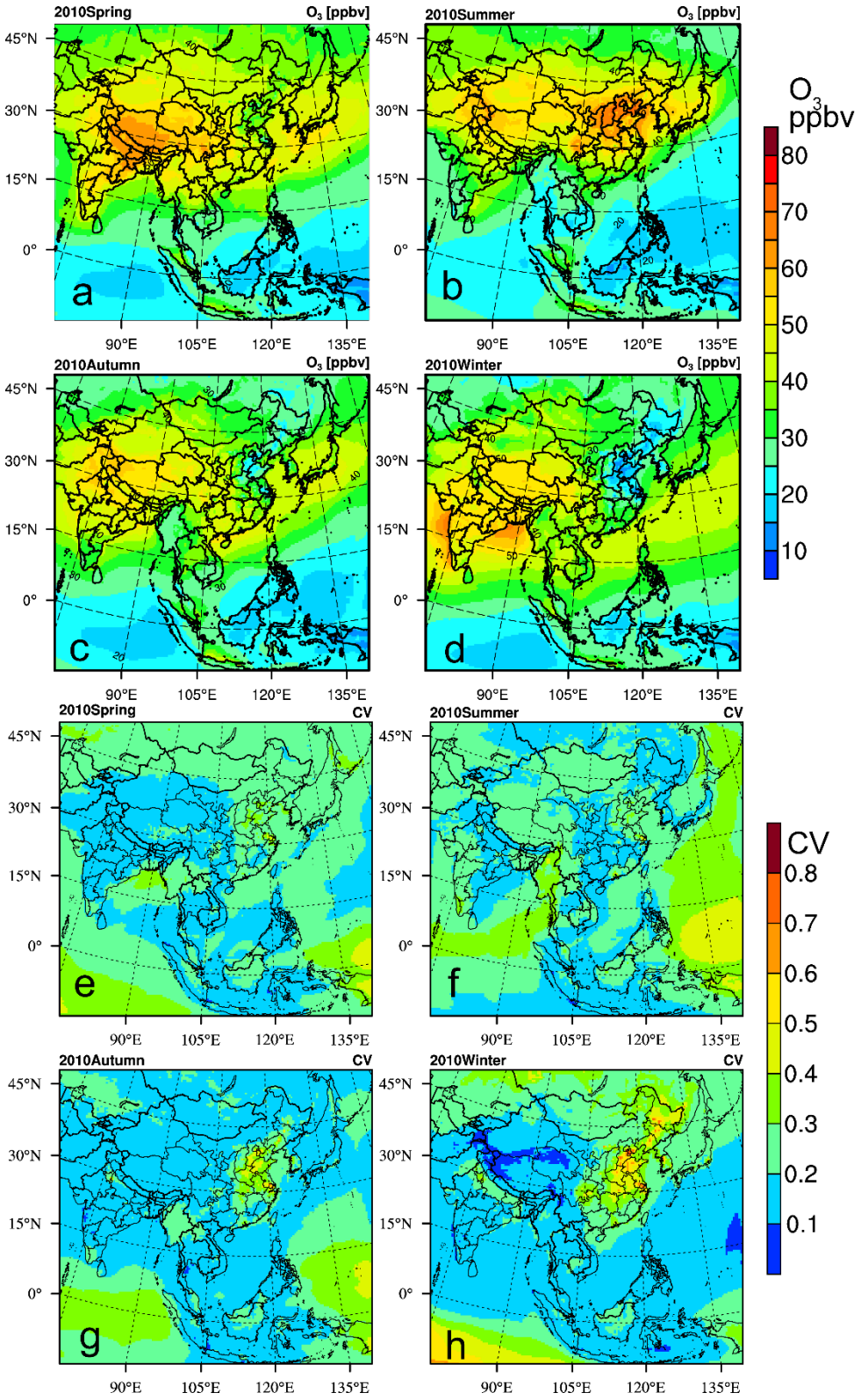

Fig.6 Li et al., 2018

.

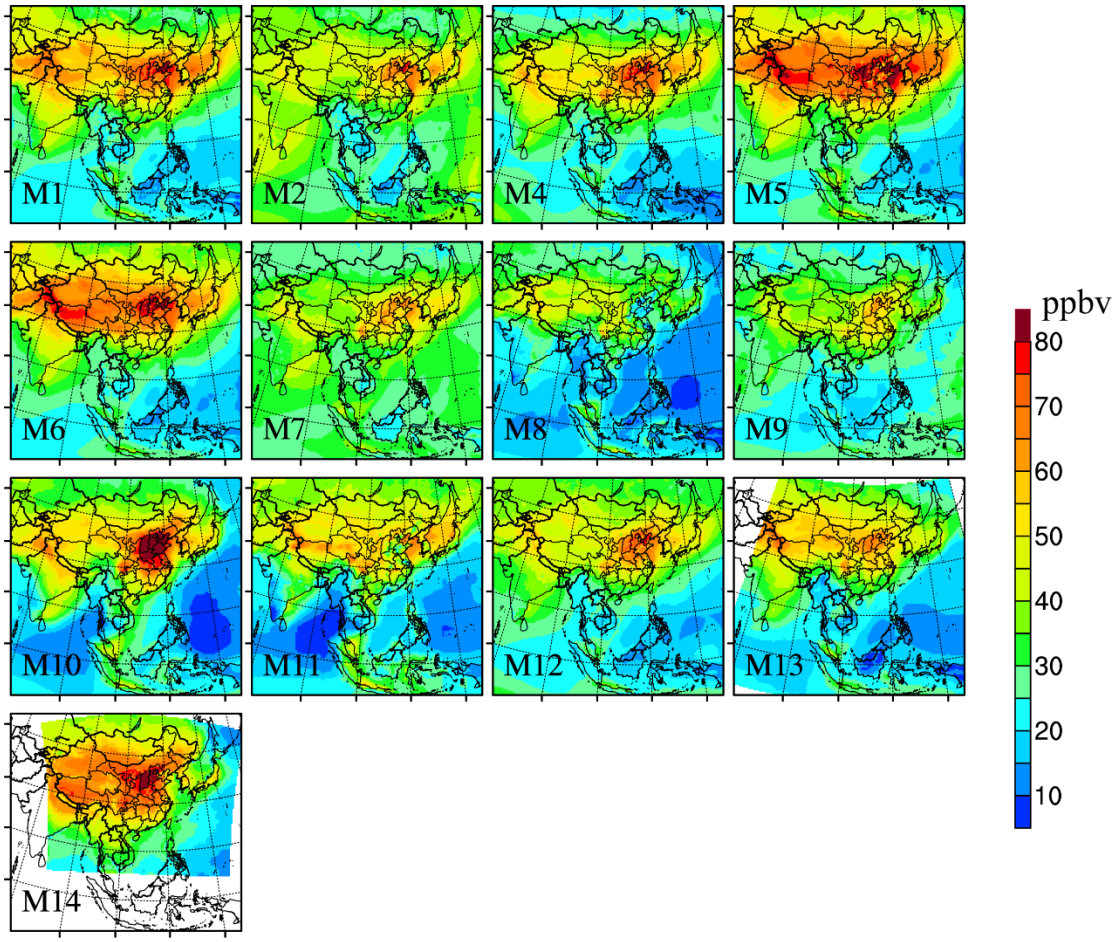

Fig.7 Li et al., 2018

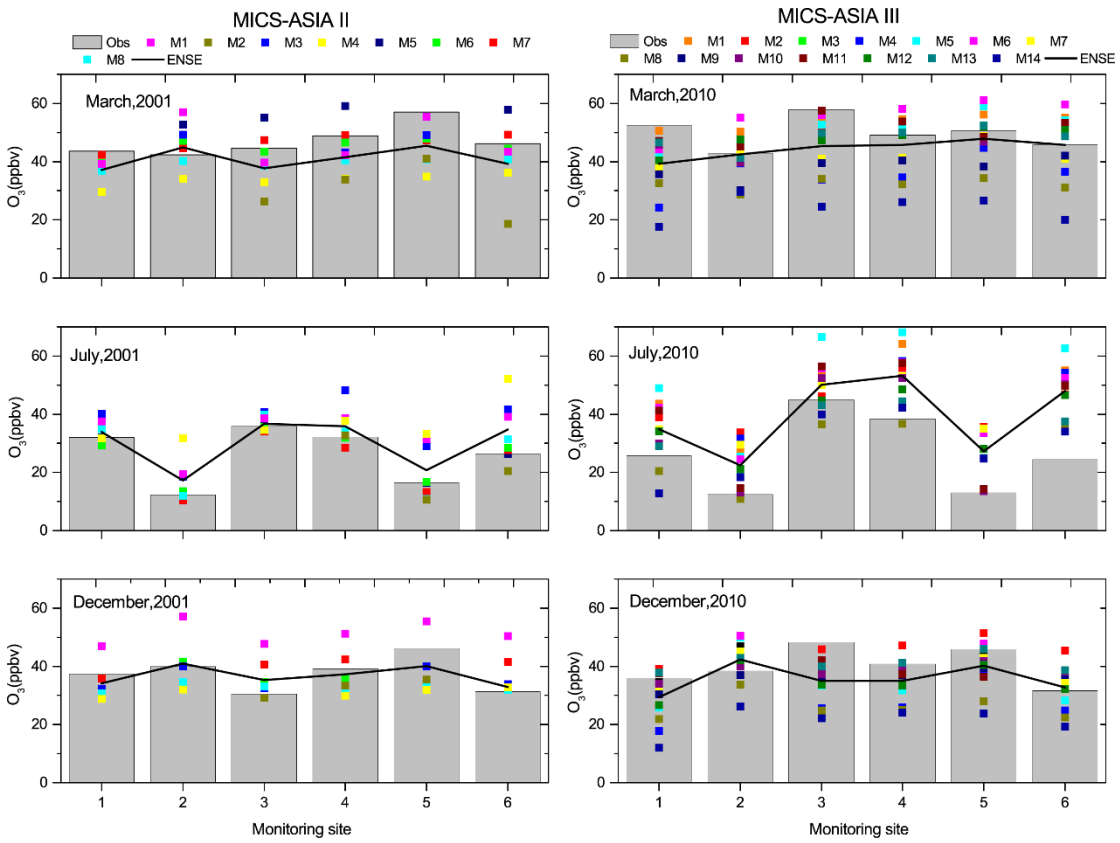

Fig.8 Li et al., 2018

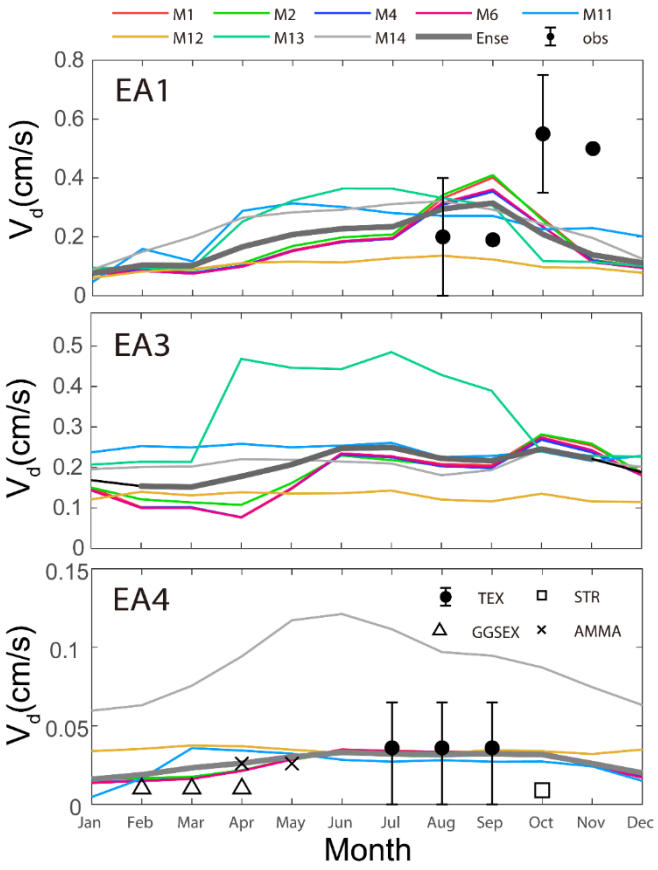

Fig.9 Li et al., 2018

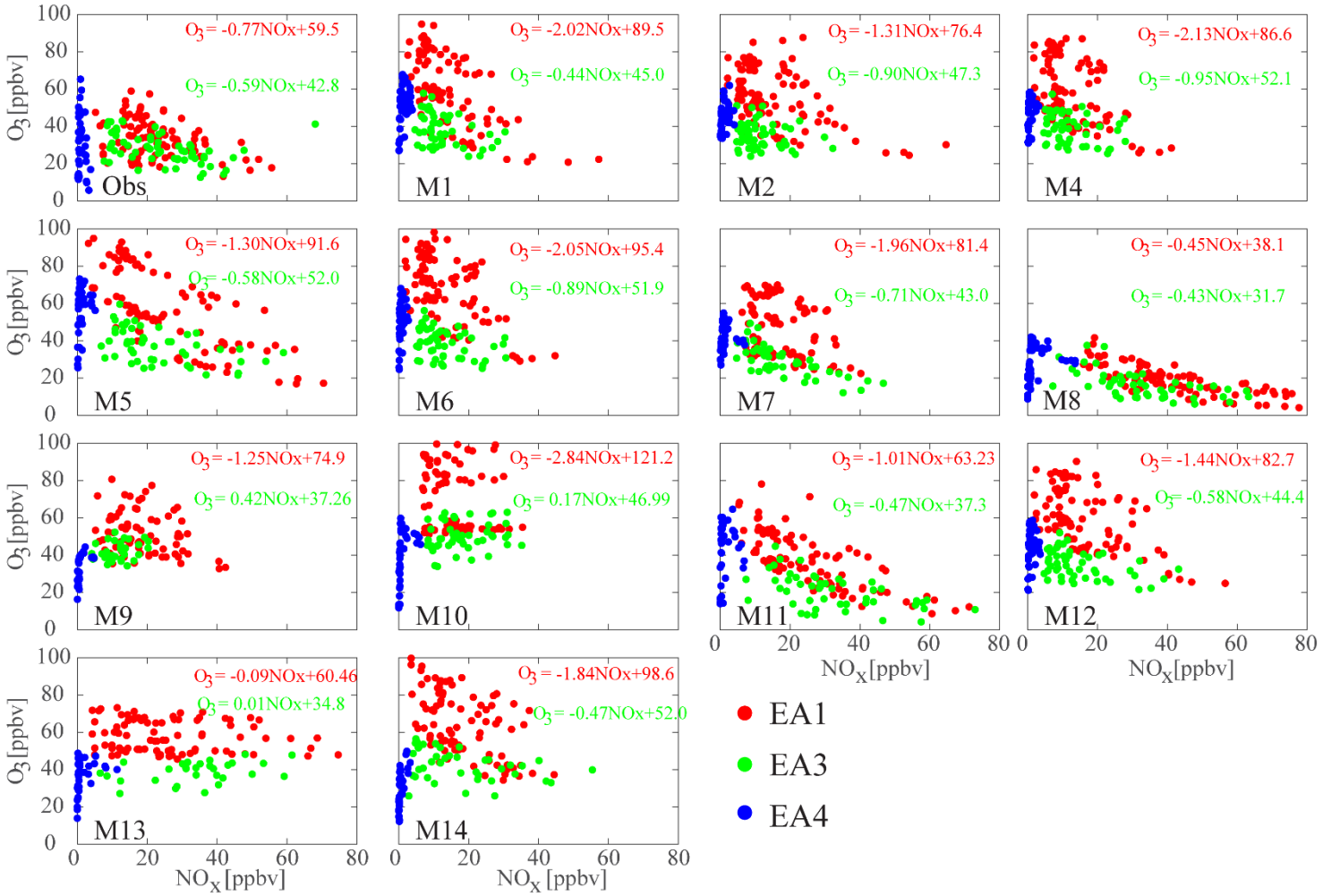

Fig.10 Li et al., 2018